Supplementary Information (SI) for Chemical Science.
This journal is © The Royal Society of Chemistry 2024

Electronic Supplementary Information

Quadrupolar Dinuclear Hypervalent Tin(IV) Compounds with Near-infrared Emission Consisting of Schiff Base Based on π-Conjugated Scaffolds

Kazuya Tanimura, Kento Tanaka, Masayuki Gon and Kazuo Tanaka*

Department of Polymer Chemistry, Graduate School of Engineering, Kyoto University Katsura, Nishikyo-ku, Kyoto 615-8510, Japan

E-mail: tanaka@poly.synchem.kyoto-u.ac.jp

Contents page

General S–3

Materials S–4

Synthetic procedures and characterization

Synthesis of **Br** S–5

Synthesis of **TPhBr** S–7

Synthesis of **TPhCN** S–10

Synthesis of **TPhCNBr** S–13

Synthesis of **TPhNC** S–16

Synthesis of **TPhNCBr** S–20

Synthesis of **P-TPh** S–24

Synthesis of **P-TPhCN** S–27

Synthesis of **P-TPhNC** S–30

Stability test by time-dependent absorption spectra S–33

Single crystal X-ray structure analysis

Analysis of **TPhCN** S–35

Analysis of **TPhNC** S–37

Computational details in **Azm**, **AzmOMe**, and **TPh** S–39

Computational details in **TPhCN** and **TPhNC** S–42

Cyclic Voltammetry S–46

Fluorescence in Solid state of TPh derivatives S–47

Solvent effects of TPh derivatives S–48

Computational details for theoretical calculation for solvent effects S–49

Solvent-dependent optical properties of polymers S–50

Optical properties of polymers in film state S–52

Computational details in **P-TPh**, **P-TPhCN**, and **P-TPhNC** S–53

Reference S–56

General

^{1}H, ^{13}C{^{1}H}, and ^{119}Sn NMR spectra were recorded on JEOL ECZ400 instruments at 400, 100, and 149 MHz, at room temperature, respectively. High-resolution ^{13}C{^{1}H} NMR spectra were recorded on an ECZ600R instrument at 150 MHz. Samples were analyzed in $CDCl_3$ and DMSO-d_6. The chemical shift values were expressed relative to Me_4Si for ^{1}H and ^{13}C{^{1}H} NMR as an internal standard in $CDCl_3$, DMSO for ^{1}H and ^{13}C{^{1}H} NMR as an internal standard in DMSO-d_6, and Me_4Sn for ^{119}Sn NMR as an external standard. High-resolution mass (HRMS) spectrometry was performed at the Technical Support Office (Department of Synthetic Chemistry and Biological Chemistry, Graduate School of Engineering, Kyoto University), and the HRMS spectra were obtained on a Thermo Fisher Scientific EXACTIVE spectrometer for electrospray ionization (ESI) and a Bruker Daltonics ultrafleXtreme for matrix-assisted laser desorption ionization (MALDI). Gel permeation chromatography (GPC) was carried out on a SHIMADZU Prominence system equipped with three consecutive polystyrene gel columns (TSK gels: G4000H_{XL}, G3000H_{XL}, G2500H_{XL}) using chloroform as an eluent after calibration with standard polystyrene samples (1.0 mL/min) at 40 ºC. UV–vis absorption spectra were recorded on a SHIMADZU UV-3600i plus spectrophotometer, and samples were analyzed at room temperature. Fluorescence emission spectra were recorded on a HORIBA Scientific Fluorolog-3 spectrofluorometer, and samples were analyzed at room temperature with PMT P928 (250~810 nm) and DSS-IGA (810~1550 nm) as detectors. Absolute photoluminescence (PL) quantum efficiency (Φ_{PL}) was recorded on a Hamamatsu Photonics Quantaurus-QY Plus C13534-01 equipped with infrared measurement unit C13684-01 using an integrating sphere; excitation was carried out using high-output xenon lamp unit L13685-01 with near-infrared cut filter and band-path filter A13686-525 (center wavelength: 525 nm, FWHM: 50 nm). Cyclic voltammetry (CV) was carried out on a BASALS-Electrochemical-Analyzer Model 600D with a grassy carbon working electrode, a Pt counter electrode, an Ag/AgCl reference electrode, and the ferrocene/ferrocenium (Fc/Fc^{+}) external reference at a scan rate of 0.1 V s^{-1}. Elemental analyses were performed at the Microanalytical Center of Kyoto University. X-ray crystallographic analysis was carried out by Rigaku Saturn 724+ with MicroMax-007HF CCD diffractometer with Varimax Mo optics using graphite-monochromated MoKα radiation. A symmetry-related absorption correction was carried out by using the program REQAB.[1] The structures were solved with SHELXT 2018/2[2,3] and refined on F^2 with SHELXL 2018/3[3–5] on YadokariXG.[6] The program ORTEP3[7] and Mercury-4.2.0 were used to generate the X-ray structural diagram.

Materials

Commercially available compounds used without purification:

Salicylaldehyde (**1**) (FUJIFILM Wako Pure Chemical Corporation)

4-Bromosalicylaldehyde (**1Br**) (Tokyo Chemical Industry Co., Ltd.)

2,5-Diaminohydroquinone dihydrochloride (**2**) (FUJIFILM Wako Pure Chemical Corporation)

2-Aminophenol (**3**) (Tokyo Chemical Industry Co., Ltd.)

2-Amino-5-bromophenol (**3Br**) (BLD Pharmatech Ltd.)

2,5-Dihydroxyterephthalaldehyde (**4**) (Tokyo Chemical Industry Co., Ltd.)

$Pd_2(dba)_3$ (dba = dibenzylideneacetone) (Strem Chemicals Inc.)

2-Dicyclohexylphosphino-2′,4′,6′-triisopropylbiphenyl (XPhos) (Strem Chemicals Inc.)

Commercially available compounds used with purification:

Diphenyltin(IV) oxide (Sigma Aldrich Co., LLC)

Diphenyltin(IV) oxide was washed with hot $CHCl_3$ before each reaction.

Commercially available solvents:

EtOH (FUJIFILM Wako Pure Chemical Corporation), acetone (deoxidized grade, FUJIFILM Wako Pure Chemical Corporation), $CHCl_3$ (FUJIFILM Wako Pure Chemical Corporation), toluene (deoxidized grade, FUJIFILM Wako Pure Chemical Corporation), CH_3CN (FUJIFILM Wako Pure Chemical Corporation) were used without purification as received.

Compounds prepared as described in the literature:

5,5′-Bis(trimethylstannyl)-3,3′-didodecyl-2,2′-bithiophene (**BT**)[8]

Compound **TPh** [9]

Synthetic procedures and characterization

Synthesis of **Br**

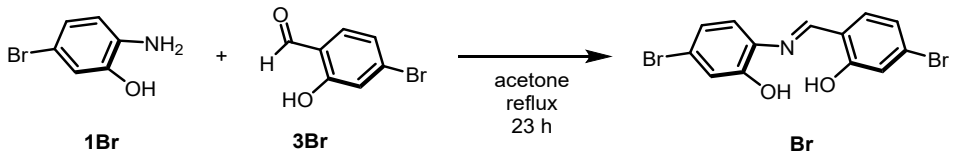

In a 50 mL round-bottom flask, 4-bromosalicylaldehyde (**1Br**, 0.935 g, 4.97 mmol, 1 equiv.), 2-amino-5-bromophenol (**3Br**, 1.000 g, 4.97 mmol, 1 equiv.) and 30 mL of ethanol were added. The solution was refluxed for 23 h. After filtration, **Br** was obtained as an orange solid (1.695 g, 4.57 mmol, 92%).

Characterization:

^{1}H NMR ($CDCl_3$, 400 MHz) δ 10.38 (br, 2H), 8.98 (s, 1H), 7.55 (d, J = 8.2 Hz, 1H), 7.35 (d, J = 8.7 Hz, 1H), 7.15–7.11 (m, 3H), 7.06 (dd, J = 8.5, 2.1 Hz, 2H) ppm; ^{13}C{^{1}H} NMR ($CDCl_3$, 100 MHz) δ 162.0, 161.1, 152.3, 133.8, 133.8, 126.3, 122.3, 121.8, 121.1, 120.0, 119.7, 119.1, 118.6 ppm; HRMS (ESI) calcd. for $C_{13}H_9Br_2NO_2$ $[M-H]^-$: 367.8927, found: 369.8927.

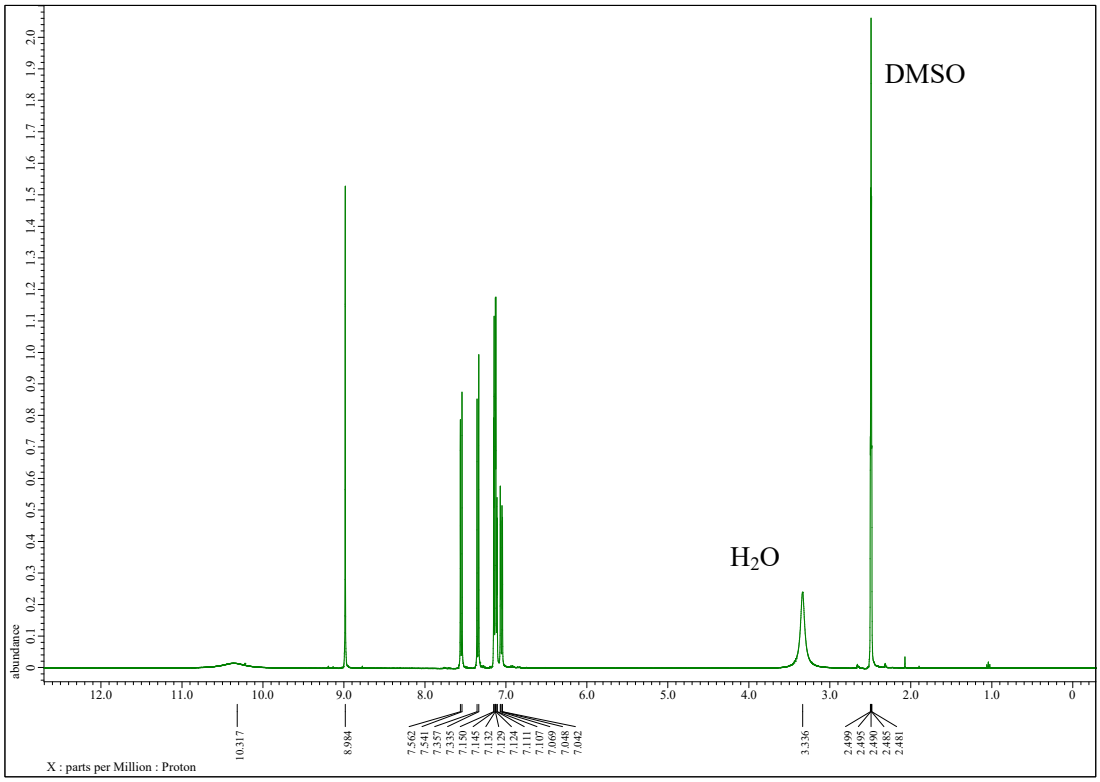

Chart S1. ^{1}H NMR spectrum of **Br** in DMSO-d_6.

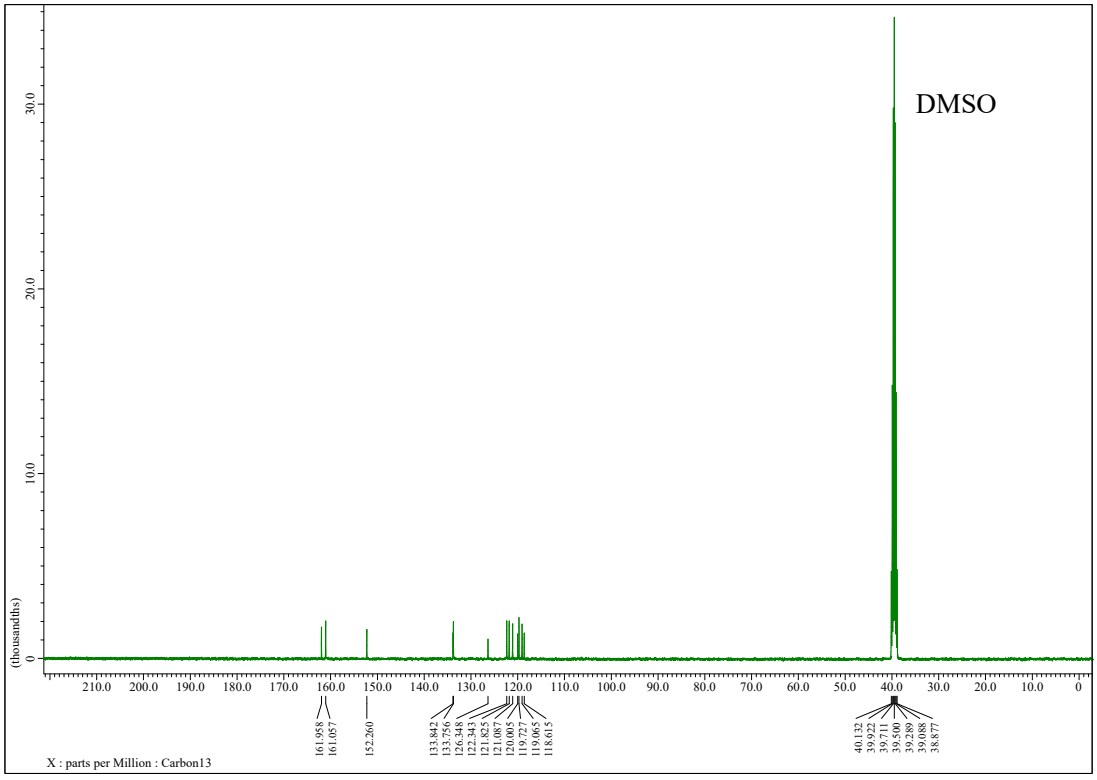

Chart S2. ^{13}C{^{1}H} NMR spectrum of **Br** in DMSO-d_6.

Synthesis of **TPhBr**

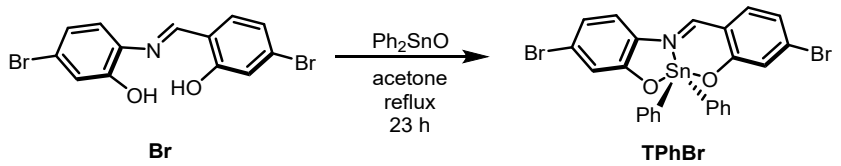

In a 50 mL round bottom flask, (*E*)-5-bromo-2-((4-bromo-2-hydroxybenzylidene)amino)phenol (**Br**) (0.500 g, 1.35 mmol, 1 equiv.), diphenyltin(IV) oxide (0.584 g, 2.02 mmol, 1.5 equiv.) and 20 mL of acetone were added under N_2. Then, the solution was refluxed for 23 h. After adding a large amount of $CHCl_3$, the mixture was filtered to remove unreacted diphenyltin(IV) oxide, and then, the solvent of the filtrate was removed with a rotary evaporator. After reprecipitation with $CHCl_3$ and EtOH, **TPhBr** was obtained as an orange solid (0.683 g, 0.106 mmol, 79%).

Characterization:

^{1}H NMR ($CDCl_3$, 400 MHz) δ 8.58 (t, $J_{H–Sn}$ = 27.4 Hz, 2H), 7.98–7.76 (m, 4H), 7.47–7.38 (m, 6H), 7.30 (dd, J = 22.6, 2.1 Hz, 2H), 7.15 (d, J = 8.7 Hz, 1H), 7.07 (d, J = 8.7 Hz, 1H), 6.91 (dd, J = 8.5, 2.1 Hz, 2H), 6.83 (dd, J = 8.7, 2.3 Hz, 2H) ppm; ^{13}C{^{1}H} NMR ($CDCl_3$, 100 MHz) δ 169.3, 160.8, 159.6, 138.9, 136.4, 136.1, 132.7, 130.6, 130.3, 128.9, 125.7, 124.1, 122.1, 121.4, 120.0, 116.8, 115.7 ppm; ^{119}Sn NMR ($CDCl_3$, 149 MHz) δ −324.9 ppm; HRMS (ESI) calcd. for $C_{25}H_{17}Br_2NO_2SnCl$ $[M+Cl]^-$: 675.8316, found: 675.8324. Elemental analysis calcd. for $C_{25}H_{17}NO_2Sn$: C 46.78 H 2.67 N 2.18, found: C 46.58 H 2.67 N 2.37.

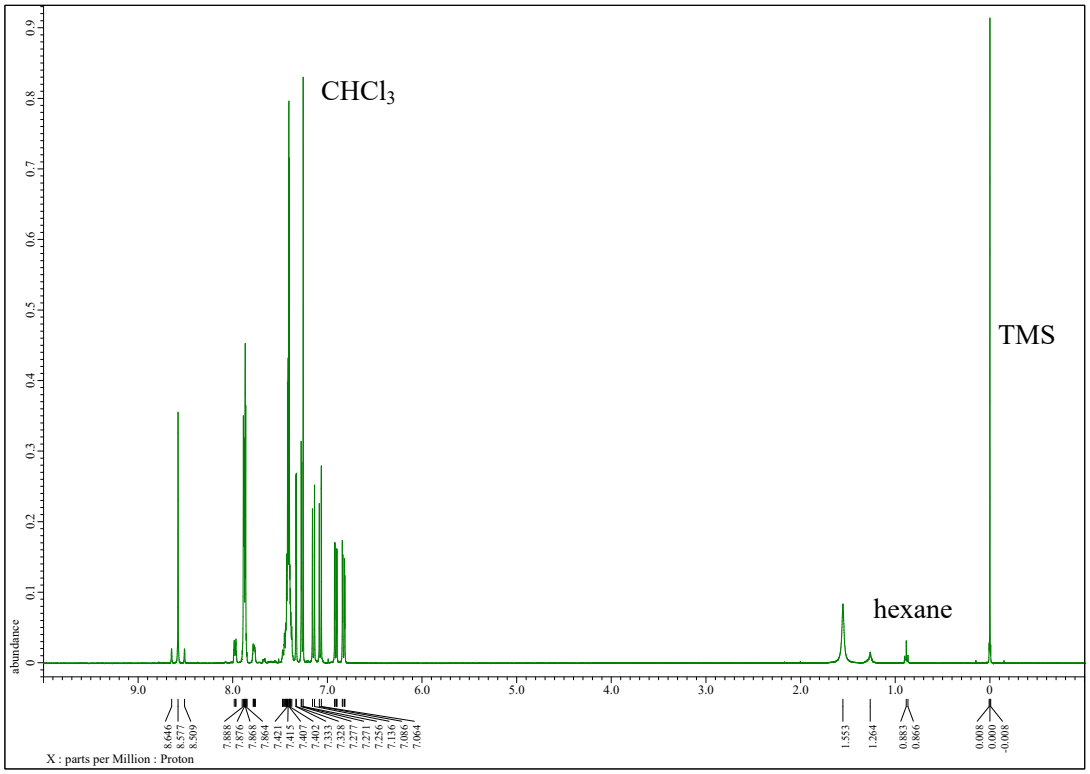

Chart S3. ^{1}H NMR spectrum of **TPhBr** in $CDCl_3$.

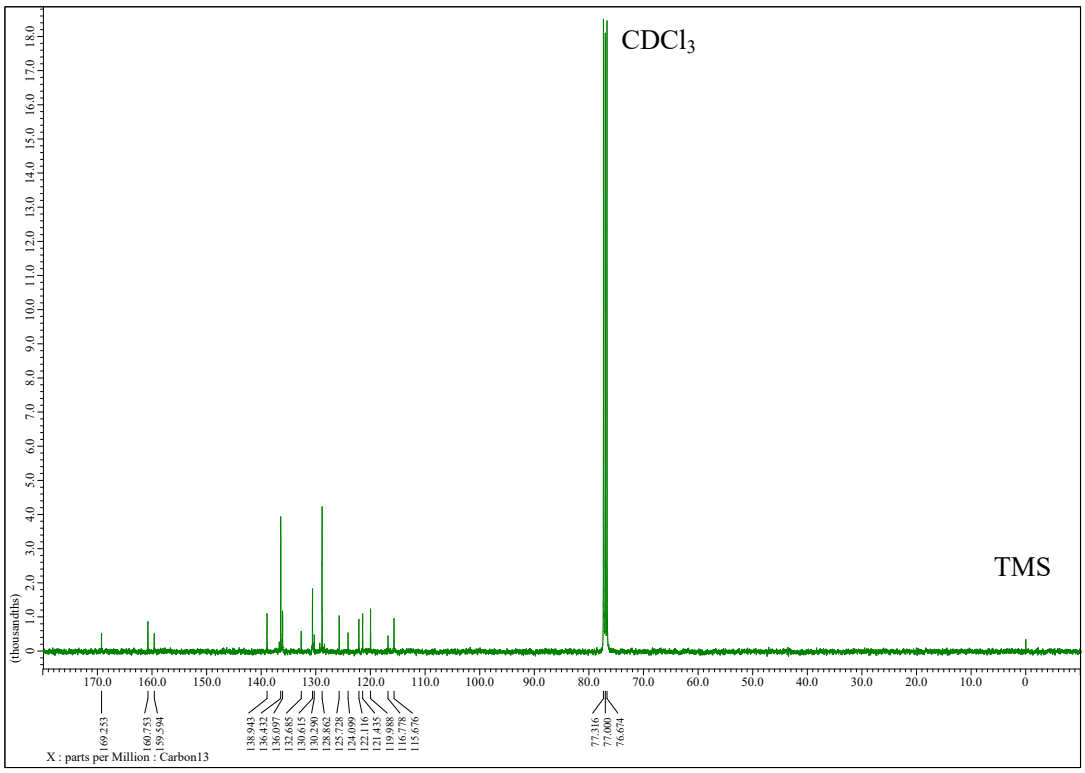

Chart S4. ^{13}C{^{1}H} NMR spectrum of **TPhBr** in $CDCl_3$.

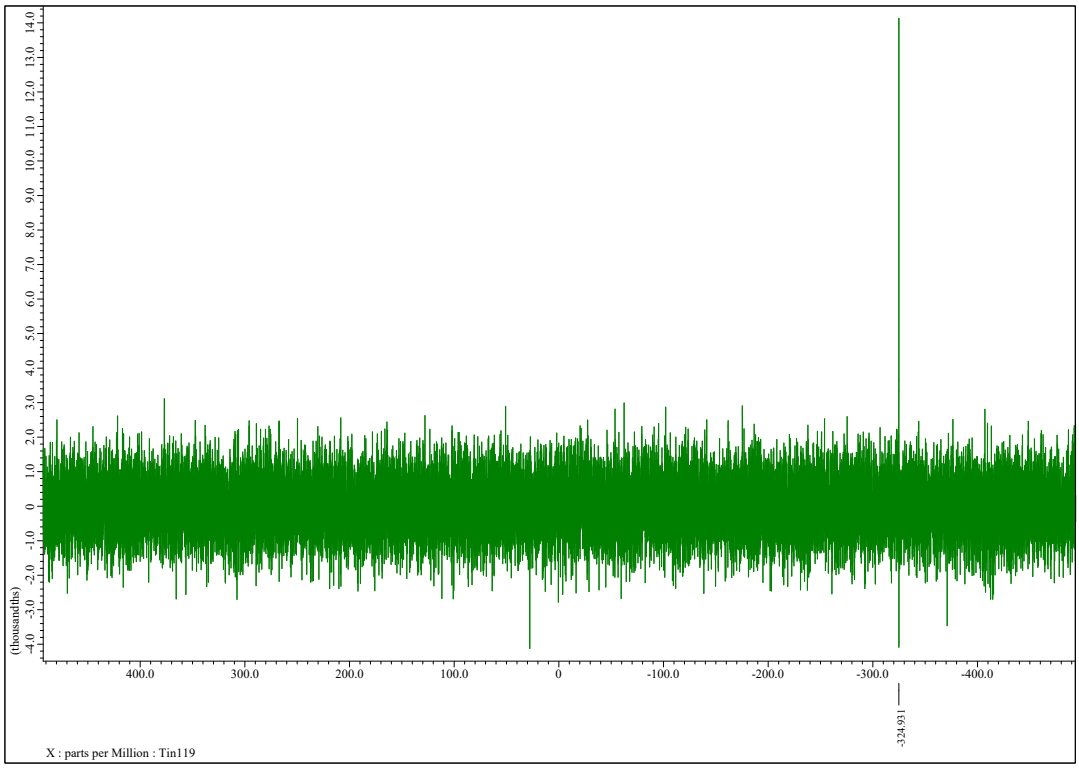

Chart S5. ^{119}Sn NMR spectrum of **TPhBr** in $CDCl_3$.

Synthesis of **TPhCN**

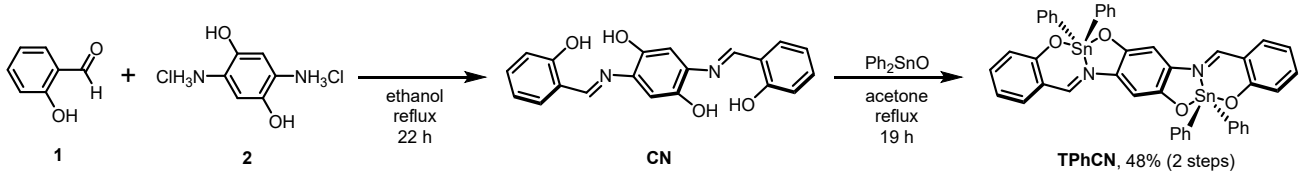

In a 30 mL round bottom flask, **1** (0.602 g, 4.93 mmol, 2.1 equiv.), **2** (0.500 g, 2.35 mmol, 1 equiv.) and 5 mL of ethanol were added. Then, the solution was stirred at 90 °C for 22 h. After cooling to −20 °C, the precipitation was collected by filtration and dried in vacuo to give **CN** as a dark red solid. The crude product was used in the next step without further purification (0.863 g).

In a 50 mL round bottom flask, **CN** (0.299 g, 0.861 mmol, 1 equiv.), diphenyltin(IV) oxide (0.623 g, 2.15 mmol, 2.5 equiv.) and 20 mL of acetone were added under N_2. Then, the solution was stirred at 70 °C for 19 h. After adding a large amount of $CHCl_3$, the mixture was filtered to remove unreacted diphenyltin(IV) oxide, and then, the solvent of the filtrate was removed with a rotary evaporator. After reprecipitation with $CHCl_3$ and CH_3CN, **TPhCN** was obtained as a black solid (0.345 g, 0.388 mmol, 48%, two steps from **1**). The single crystal was collected by solution diffusion method with CH_2Cl_2 as a good solvent and acetonitrile as a poor solvent.

Characterization:

^{1}H NMR ($CDCl_3$, 400 MHz) δ 8.67 (t, $J_{H–Sn}$ = 28.2 Hz, 2H), 8.05–7.79 (m, 8H), 7.49 (ddd, J = 8.4, 7.2, 2.0 Hz, 2H), 7.45–7.33 (m, 12H), 7.26 (dd, J = 8.0, 1.6 Hz, 2H), 7.14 (s, 2H), 7.11 (d, J = 8.4 Hz, 2H), 6.83–6.77 (m, 2H) ppm; ^{13}C{^{1}H} NMR ($CDCl_3$, 100 MHz) δ 169.6, 161.3, 150.9, 139.9, 137.1, 136.5 ($J_{C–Sn}$ = 26.9 Hz), 135.4, 132.9, 130.3, 128.7($J_{C–Sn}$ = 43.2 Hz), 122.8, 118.1, 117.6, 103.3 ppm; ^{119}Sn NMR ($CDCl_3$, 149 MHz) δ −324.9 ppm; HRMS (ESI) calcd. for $C_{44}H_{32}N_2O_4Sn_2Na$ $[M+Na]^+$: 913.0292, found: 913.0297. Elemental analysis calcd. for $C_{44}H_{32}N_2O_4Sn_2$: C 59.37 H 3.62 N 3.15, found: C 59.24 H 3.67 N 3.07.

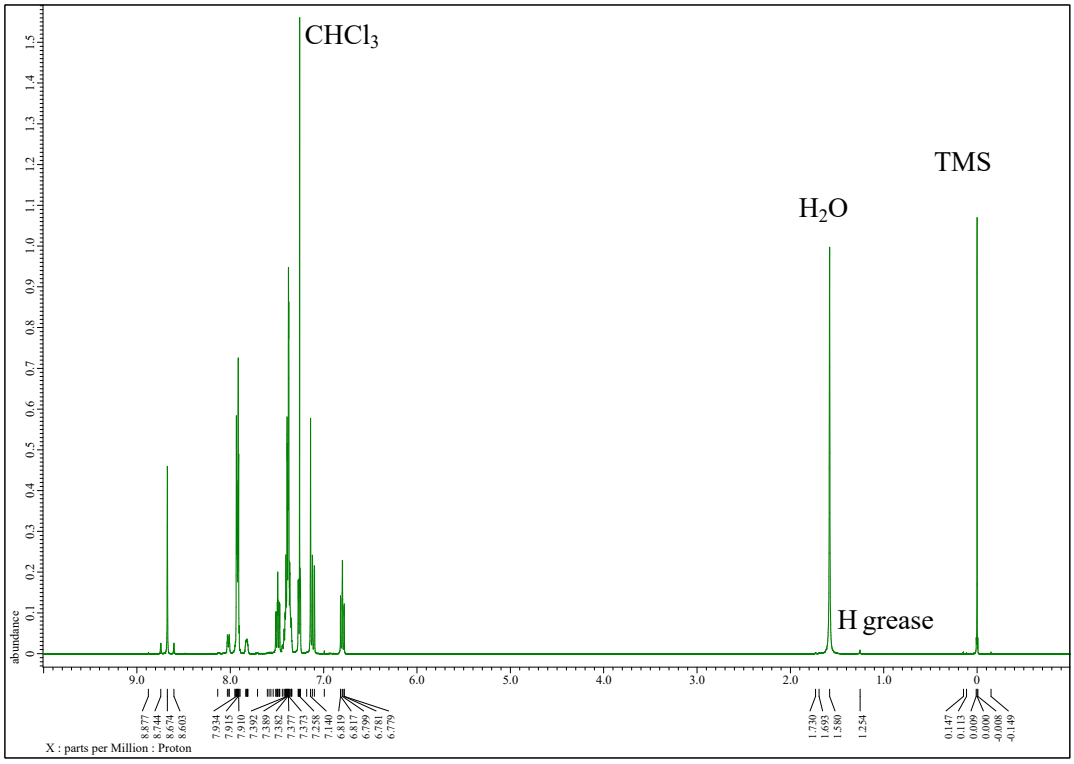

Chart S6. ^{1}H NMR spectrum of **TPhCN** in $CDCl_3$ at 400 MHz.

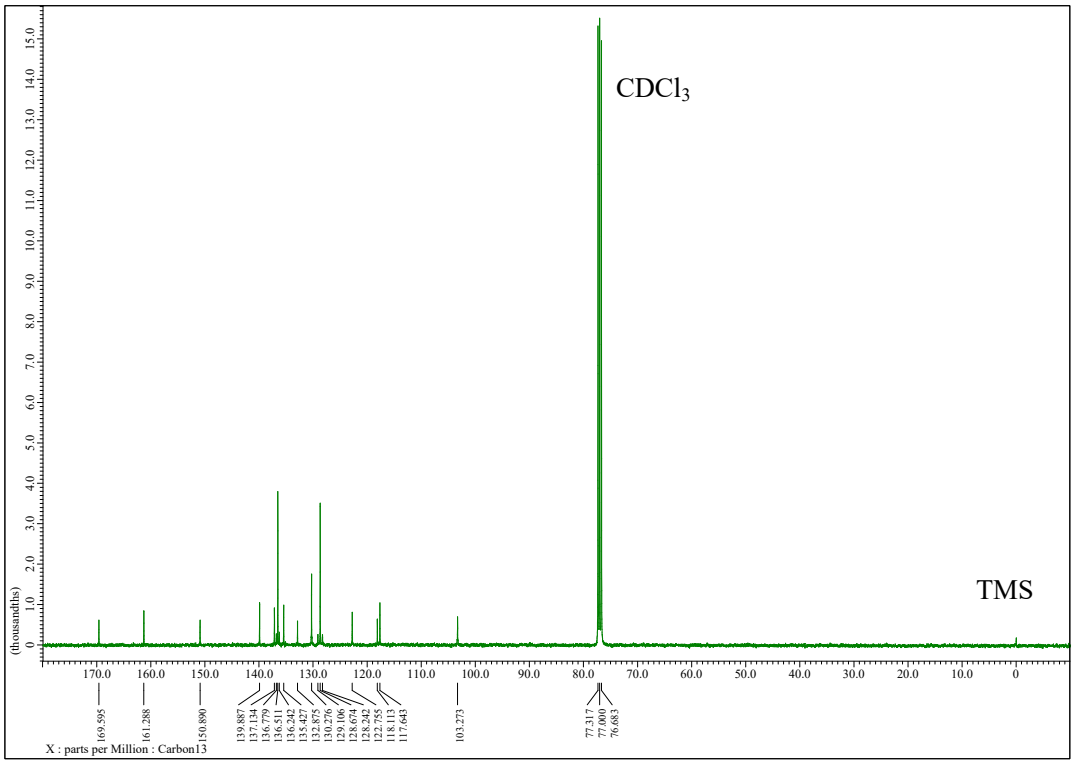

Chart S7. ^{13}C{^{1}H} NMR spectrum of **TPhCN** in $CDCl_3$ at 100 MHz.

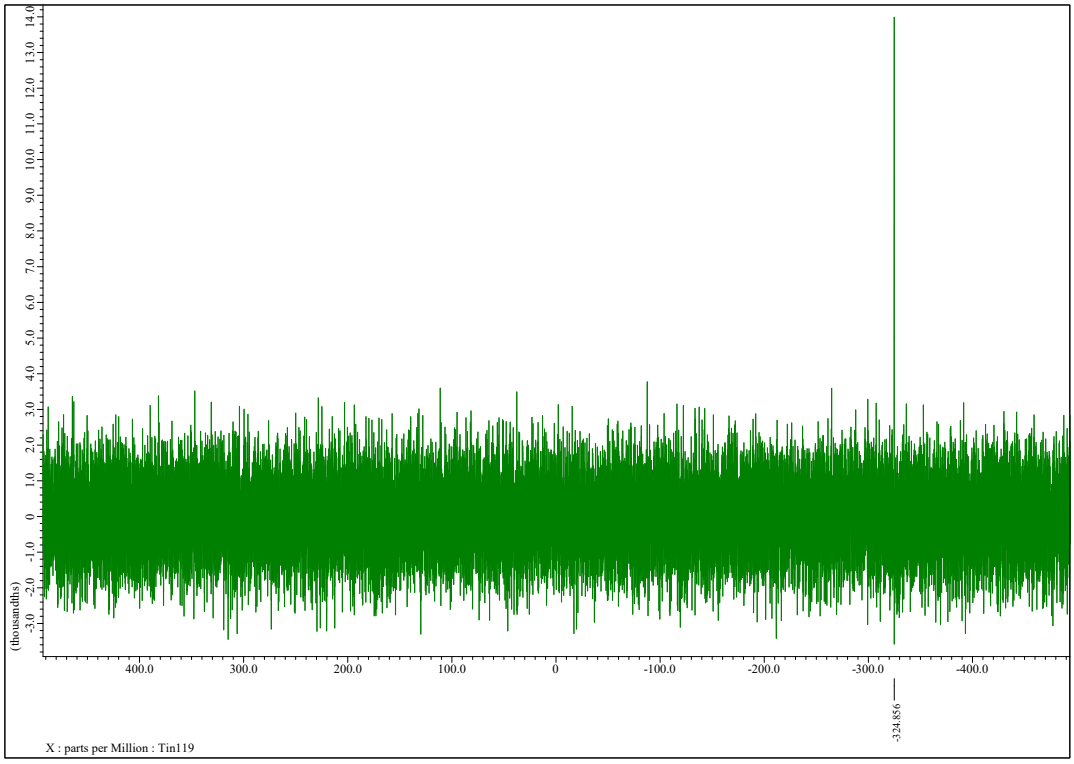

Chart S8. ^{119}Sn NMR spectrum of **TPhCN** in $CDCl_3$ at 149 MHz.

Synthesis of **TPhCNBr**

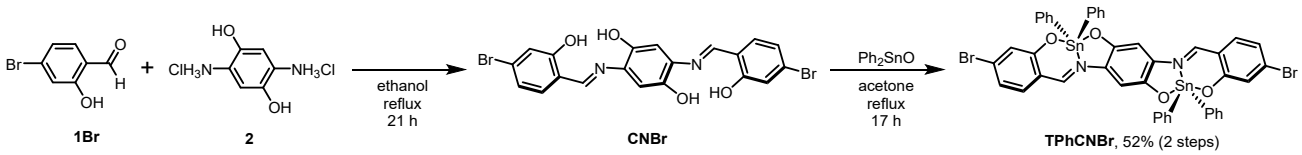

In a 20 mL round bottom flask, **1Br** (0.990 g, 4.93 mmol, 2.1 equiv.), **2** (0.500 g, 2.35 mmol, 1 equiv.) and 5 mL of ethanol were added. Then, the solution was stirred at 90 °C for 21 h. After cooling to −20 °C, the precipitation was collected by filtration and dried in vacuo to give **CNBr** as a brown solid. The crude product was used in the next step without any further purification.

In a 50 mL round bottom flask, **CNBr** (0.393 g, 0.776 mmol, 1 equiv.), diphenyltin(IV) oxide (0.560 g, 1.94 mmol, 2.5 equiv.) and 30 mL of acetone were added under N_2. Then, the solution was stirred at 70 °C for 17 h. After adding a large amount of $CHCl_3$, the mixture was filtered to remove unreacted diphenyltin(IV) oxide, and then the solvent of the filtrate was removed with a rotary evaporator. After reprecipitation with $CHCl_3$ and CH_3CN, **TPhCNBr** was obtained as a black solid (0.503 g, 0.480 mmol, 52%, two steps from **1Br**).

Characterization:

^{1}H NMR ($CDCl_3$, 400 MHz) δ 8.61 (t, $J_{H–Sn}$ = 27.2 Hz, 2H), 8.00–7.77 (m, 8H), 7.45–7.35 (m, 12H), 7.33 (d, J = 2.0 Hz, 2H), 7.11 (s, 2H), 7.10 (d, J = 8.4 Hz, 2H), 6.93 (dd, J = 8.8, 1.6 Hz, 2H) ppm; ^{13}C{^{1}H} NMR ($CDCl_3$, 150 MHz) δ 169.3, 160.5, 151.1, 139.5, 136.5 ($J_{C–Sn}$ = 27.3 Hz), 136.1, 133.0, 132.5, 130.5, 128.8 ($J_{C–Sn}$ = 43.4 Hz), 125.7, 121.4, 117.1, 103.4 ppm; ^{119}Sn NMR ($CDCl_3$, 149 MHz) δ −324.6 ppm; HRMS (ESI) calcd. for $C_{44}H_{30}Br_2N_2O_4Sn_2Na$ $[M+Na]^+$: 1070.8482, found: 1070.8494. Elemental analysis calcd. for $C_{44}H_{30}Br_2N_2O_4Sn_2$: C 50.43 H 2.89 N 2.67, found: C 50.36 H 2.79 N 2.48.

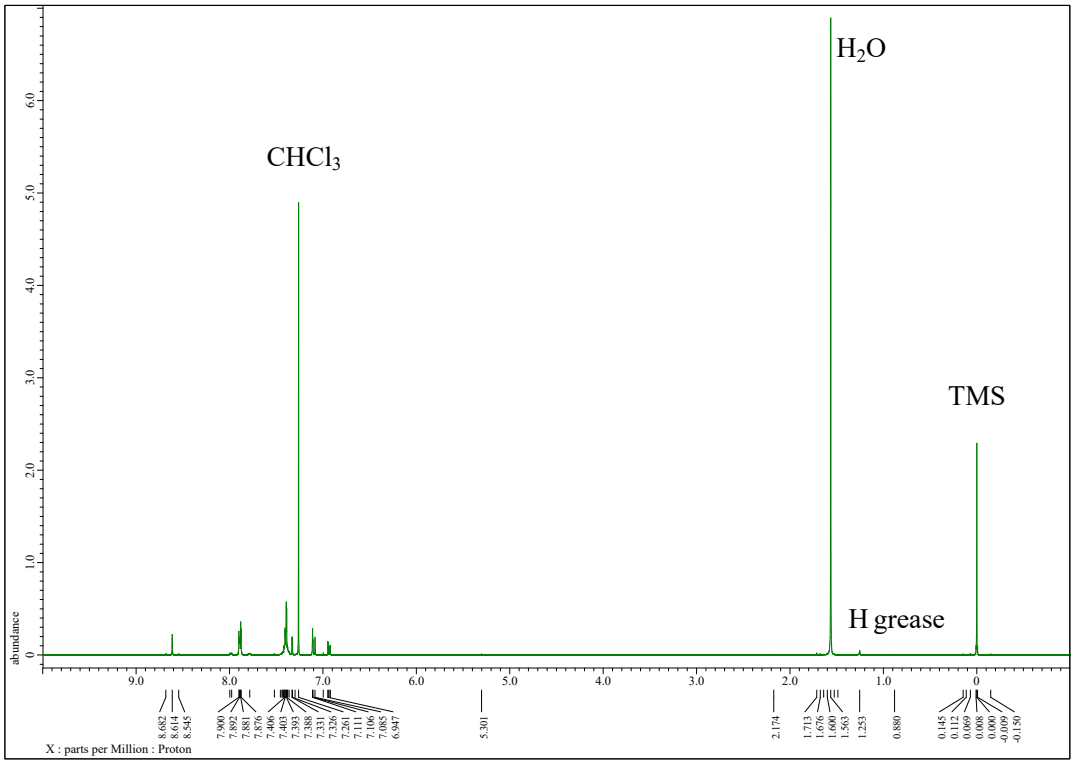

Chart S9. ^{1}H NMR spectrum of **TPhCNBr** in $CDCl_3$ at 400 MHz.

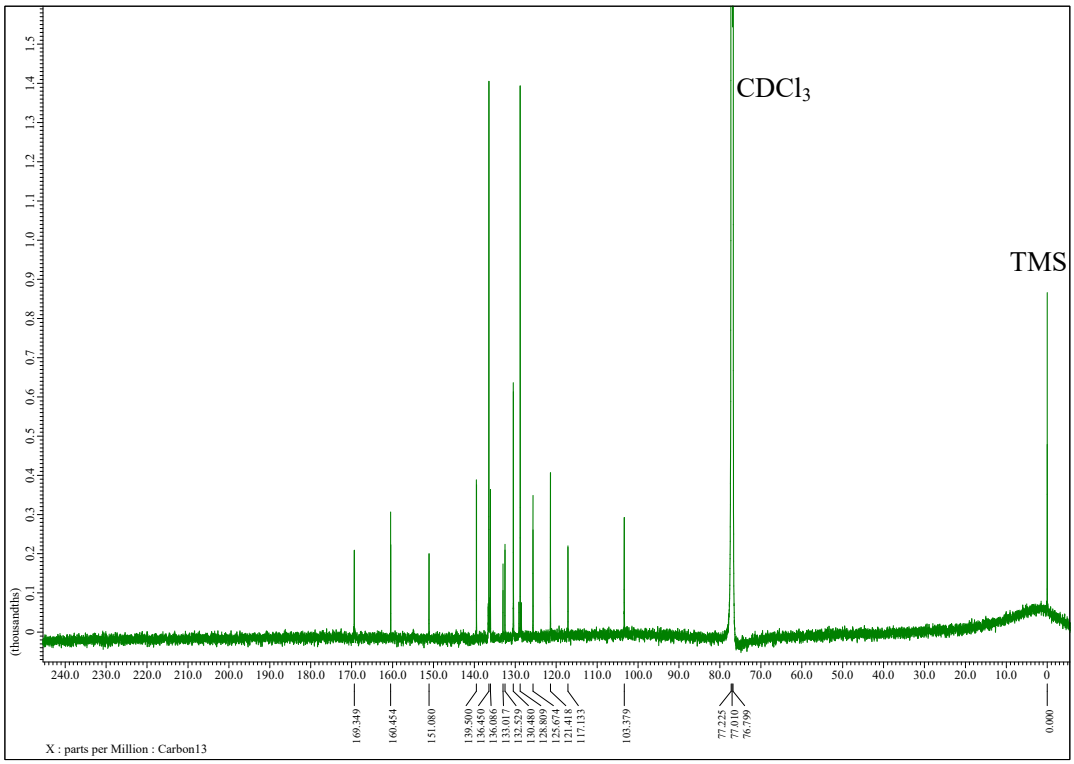

Chart S10. ^{13}C{^{1}H} NMR spectrum of **TPhCNBr** in $CDCl_3$ at 150 MHz.

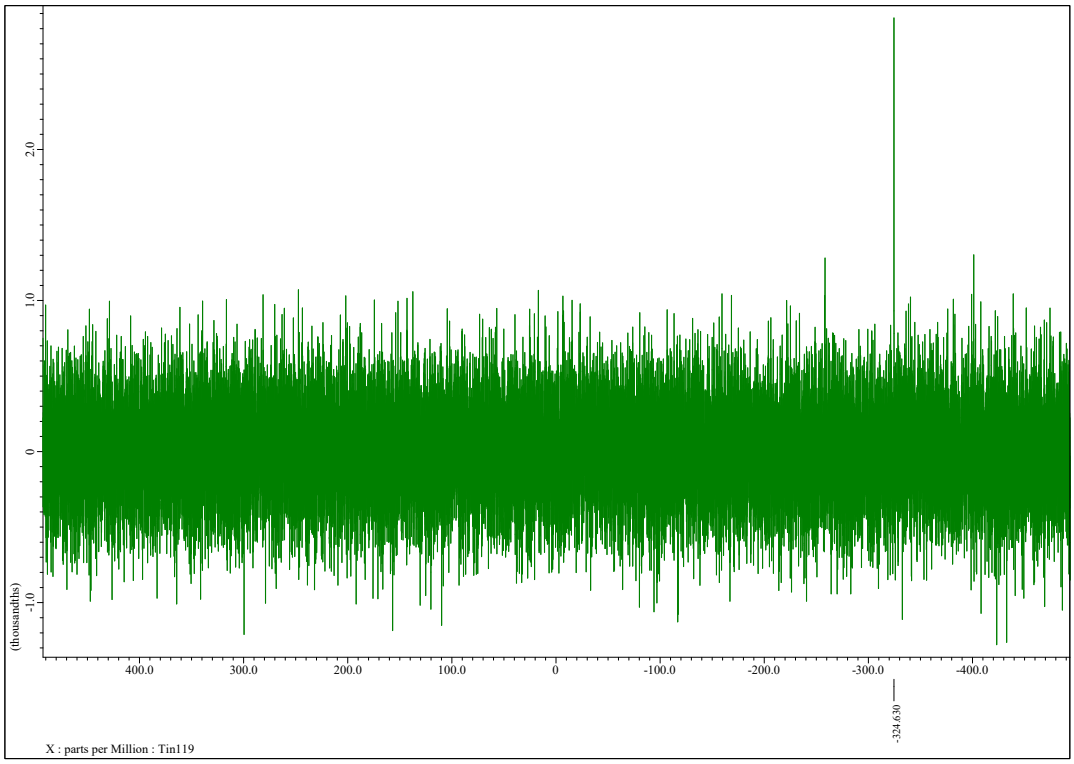

Chart S11. ^{119}Sn NMR spectrum of **TPhCNBr** in $CDCl_3$ at 149 MHz.

Synthesis of **NC** and **TPhNC**

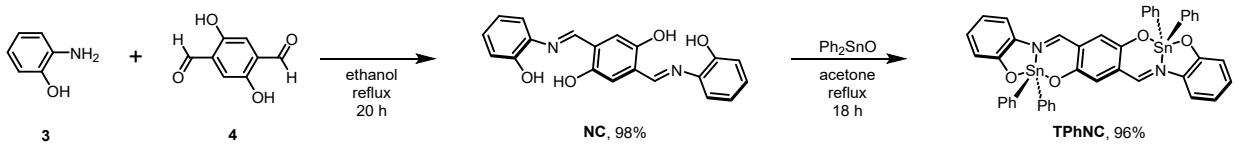

In a 20 mL round-bottom flask, **3** (0.692 g, 6.34 mmol, 2.1 equiv.), **4** (0.501 g, 3.02 mmol, 1 equiv.) and 5 mL of ethanol were added under N_2. Then, the solution was stirred at 90 °C for 20 h. After cooling to −20 °C, the precipitation was collected by filtration and dried in vacuo to give **NC** as a dark solid (1.033 g, 2.965 mmol, 98%).

Characterization:

^{1}H NMR (DMSO-d_6, 400 MHz) δ 9.78 (s, 2H), 8.96 (s, 2H), 7.37 (dd, J = 8.0, 1.6 Hz, 2H), 7.17–7.11 (m, 2H), 6.98–6.94 (m, 2H), 6.88 (td, J = 7.6, 1.6 Hz, 2H) ppm; ^{13}C{^{1}H} NMR (DMSO-d_6, 100 MHz) δ 160.6, 152.2, 151.5, 135.1, 128.5, 122.8, 119.6, 119.5, 118.4, 116.6 ppm. HRMS (EI) calcd. for $C_{20}H_{16}N_2O_4$ $[M]^+$: 348.1105, found: 348.1096. Elemental analysis calcd. for $C_{30}H_{16}N_2O_4$: C 68.96 H 4.63 N 8.04, found: C 68.90 H 4.66 N 7.85.

In a 100 mL round bottom flask, **NC** (0.303 g, 0.861 mmol, 1 equiv.), diphenyltin(IV) oxide (0.622 g, 2.15 mmol, 2.5 equiv.) and 20 mL of acetone were added under N_2. Then, the solution was stirred at 70 °C for 18 h. After adding a large amount of $CHCl_3$, the mixture was filtered to remove unreacted diphenyltin(IV) oxide. The filtrate solvent was removed with a rotary evaporator to afford **TPhNC** (0.742 g, 0.834 mmol, 96%) as a black solid. The single crystal was collected by solution diffusion method with CH_2Cl_2 as a good solvent and hexane as a poor solvent.

Characterization:

^{1}H NMR ($CDCl_3$, 400 MHz) δ 8.72 (t, $J_{H–Sn}$ = 25.6 Hz, 2H), 8.05–7.79 (m, 8H), 7.47–7.33 (m, 14H), 7.32–7.26 (m, 2H), 7.14–7.08 (m, 4H), 6.75 (t, J = 8.0 Hz, 2H) ppm; ^{13}C{^{1}H} NMR ($CDCl_3$, 100 MHz) δ 160.1, 159.8, 158.3, 139.6, 136.6 ($J_{C–Sn}$ = 26.8 Hz), 131.6, 130.9, 130.4, 128.7 ($J_{C–Sn}$ = 43.2 Hz), 125.8, 124.8, 119.5, 117.2, 115.0 ppm; ^{119}Sn NMR ($CDCl_3$, 149 MHz) δ −330.3 ppm; HRMS (ESI) calcd. for $C_{44}H_{32}N_2O_4Sn_2$ $[M+Na]^+$: 913.0292, found: 913.0298. Elemental analysis calcd. for $C_{44}H_{32}N_2O_4Sn_2$: C 59.37 H 3.62 N 3.15, found: C 59.51 H 3.58 N 3.02.

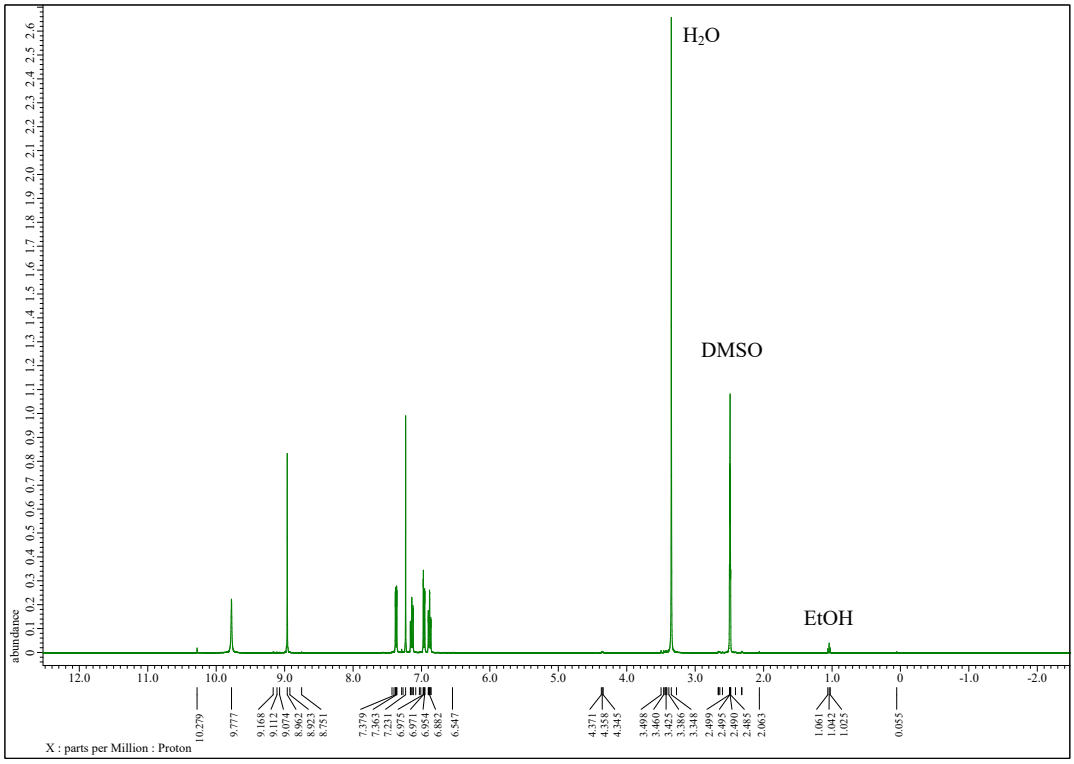

Chart S12. ^{1}H NMR spectrum of **NC** in DMSO-d_6 at 400 MHz.

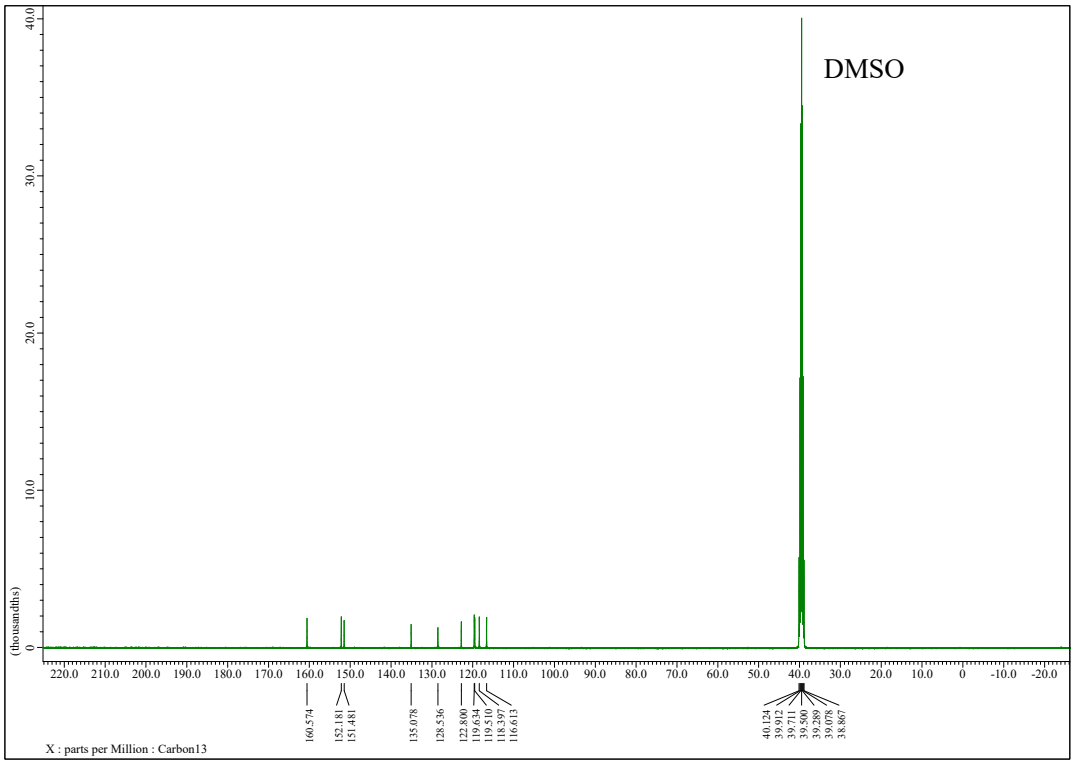

Chart S13. ^{13}C{^{1}H} NMR spectrum of **NC** in DMSO-d_6 at 100 MHz.

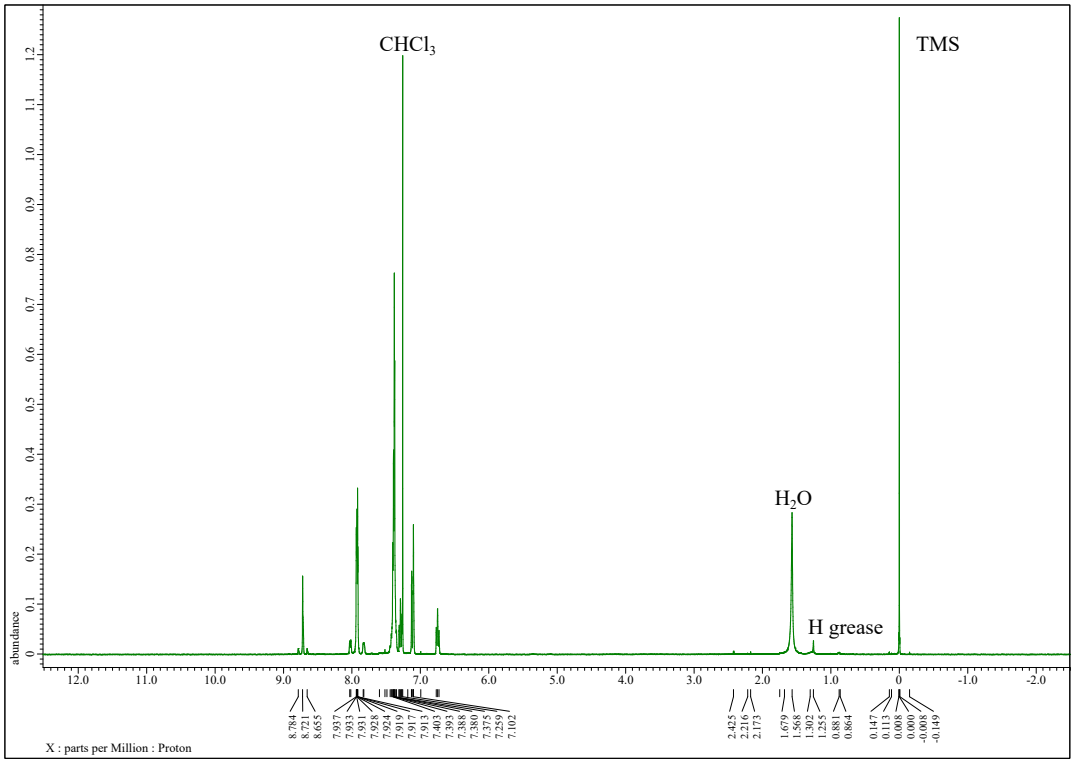

Chart S14. ^{1}H NMR spectrum of **TPhNC** in $CDCl_3$ at 400 MHz.

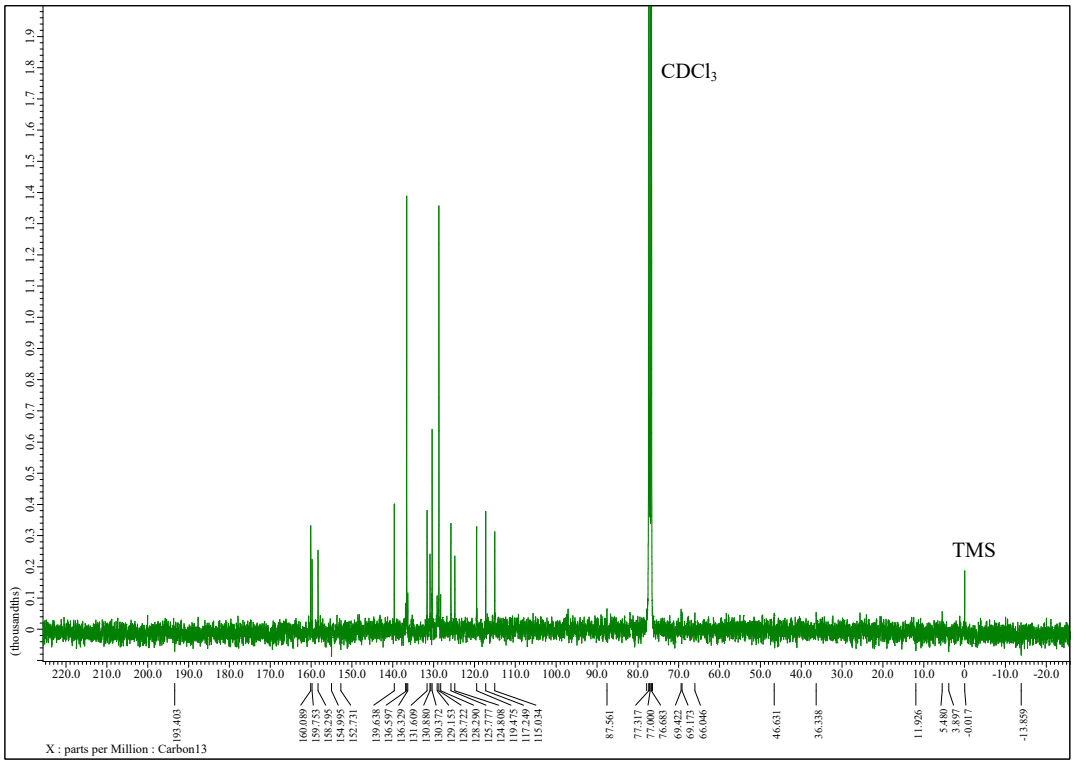

Chart S15. ^{13}C{^{1}H} NMR spectrum of **TPhNC** in $CDCl_3$ at 100 MHz.

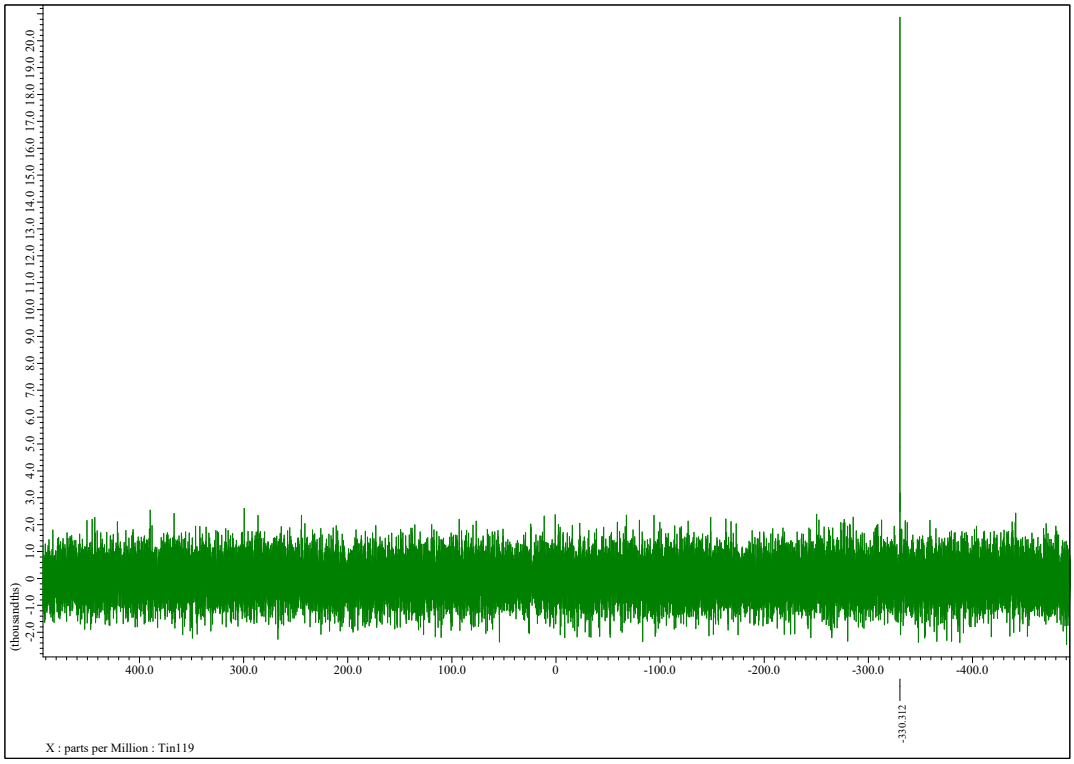

Chart S16. ^{119}Sn NMR spectrum of **TPhNC** in $CDCl_3$ at 149 MHz.

Synthesis of **NCBr** and **TPhNCBr**

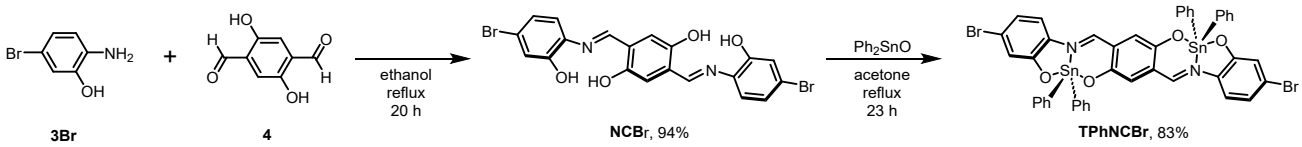

In a 20 mL round-bottom flask, **3Br** (1.14 g, 6.07 mmol, 2.1 equiv.), **4** (0.480 g, 2.89 mmol, 1 equiv.) and 5 mL of ethanol were added under N_2. Then, the solution was stirred at 90 °C for 20 h. After cooling to −20 °C, the precipitation was collected by filtration and dried in vacuo to give **NCBr** as a dark solid (1.38 g, 2.72 mmol, 94%).

Characterization:

^{1}H NMR (DMSO-d_6, 400 MHz) δ 10.30 (br, 2H), 10.28 (s, 2H), 8.96 (s, 2H), 7.33 (d, J = 8.0 Hz, 2H), 7.24 (s, 2H), 7.14 (d, J = 2.0 Hz, 2H), 7.06 (dd, J = 8.8, 2.4 Hz, 2H) ppm; ^{13}C{^{1}H} NMR (DMSO-d_6, 100 MHz) δ 161.1, 152.6, 152.1, 134.8, 123.0, 122.3, 121.3, 120.2, 119.1, 118.4 ppm; HRMS (EI) calcd. for $C_{20}H_{14}N_2O_4Br_2$ $[M]^+$: 503.9315, found: 503.9312.

In a 100 mL round bottom flask, **NCBr** (0.500 g, 0.988 mmol, 1 equiv.), diphenyltin(IV) oxide (0.714 g, 2.46 mmol, 2.5 equiv.) and 20 mL of acetone were added under N_2. Then, the solution was stirred at 70 °C for 23 h. After adding a large amount of $CHCl_3$, the mixture was filtered to remove unreacted diphenyltin(IV) oxide. The filtrate solvent was removed with a rotary evaporator to afford **TPhNCBr** (0.859 g, 0.819 mmol, 83%) as a black solid.

Characterization:

^{1}H NMR ($CDCl_3$, 400 MHz) δ 8.67 (t, $J_{H–Sn}$ = 25.2 Hz, 2H), 8.02−7.76 (m, 8H), 7.48−7.33 (m, 12H), 7.29 (d, J = 2.0 Hz, 2H), 7.21 (d, J = 8.8 Hz, 2H), 7.08 (s, 2H), 6.86 (dd, J = 8.8, 1.6 Hz, 2H) ppm; ^{13}C{^{1}H} NMR ($CDCl_3$, 150 MHz) δ 160.3, 160.2, 158.3, 139.2, 136.6 ($J_{C–Sn}$ = 26.7 Hz), 130.6, 130.2, 128.8 ($J_{C–Sn}$ = 42.3 Hz), 125.9, 125.5, 124.9, 122.5, 120.3, 116.1 ppm; ^{119}Sn NMR ($CDCl_3$, 149 MHz) δ −328.4 ppm; HRMS (ESI) calcd. for $C_{44}H_{32}N_2O_4Sn_2$ $[M+Na]^+$: 1070.8482, found: 1070.8482. Elemental analysis calcd. for $C_{44}H_{32}N_2O_4Sn_2$: C 50.43 H 2.89 N 2.67, found: C 50.31 H 2.93 N 2.55.

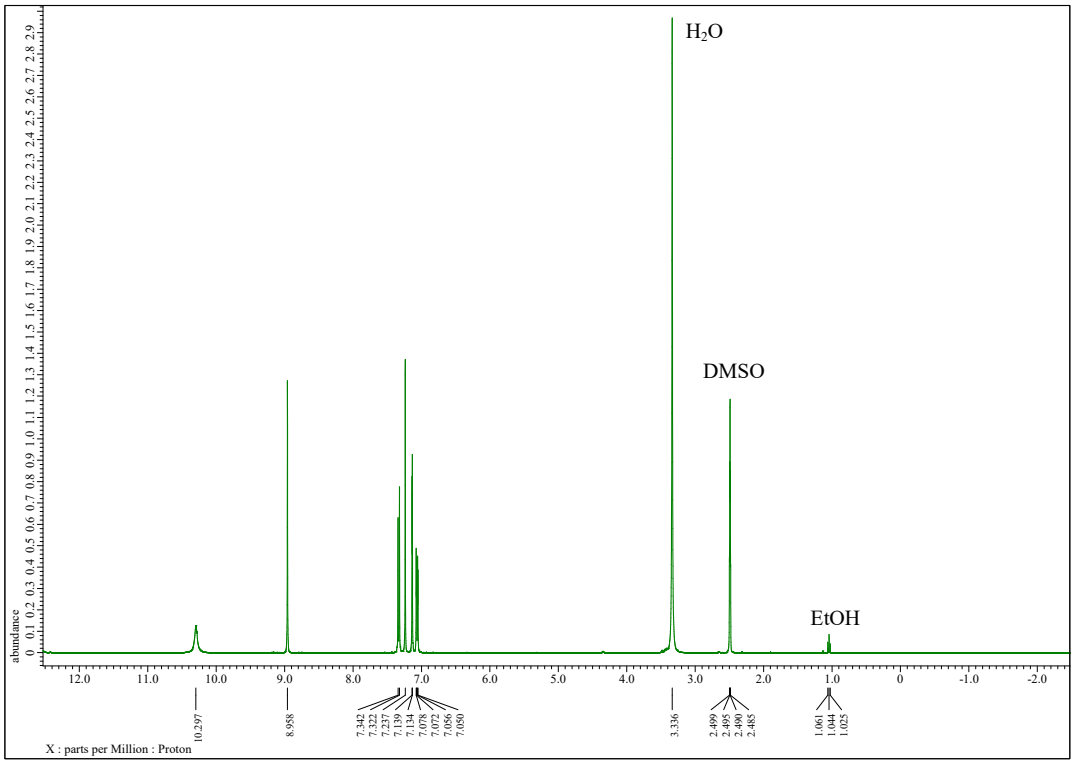

Chart S17. ^{1}H NMR spectrum of **NCBr** in DMSO-d_6 at 400 MHz.

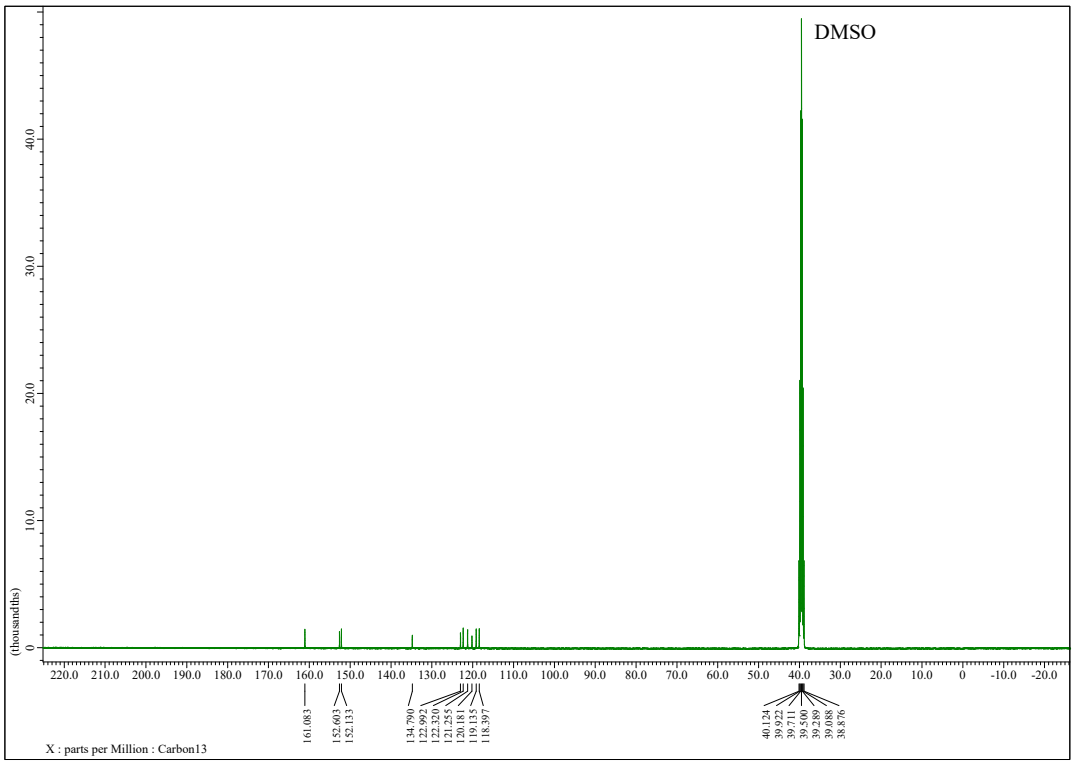

Chart S18. ^{13}C{^{1}H} NMR spectrum of **NCBr** in DMSO-d_6 at 100 MHz.

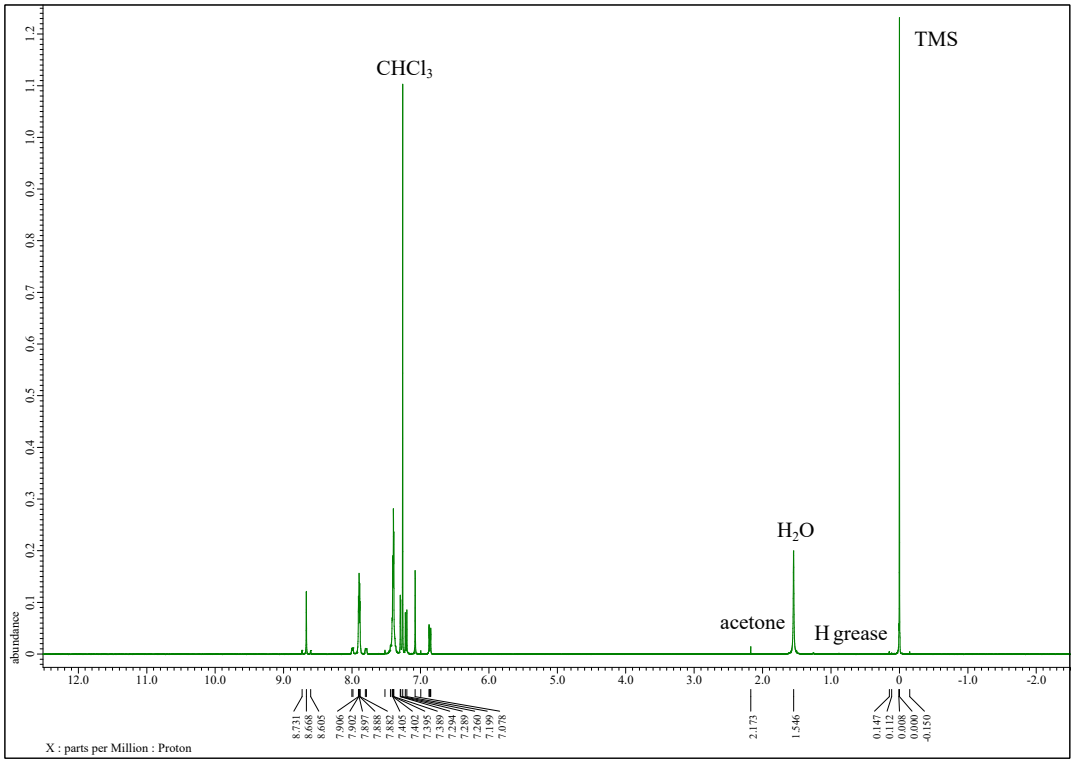

Chart S19. ^{1}H NMR spectrum of **TPhNCBr** in $CDCl_3$ at 400 MHz.

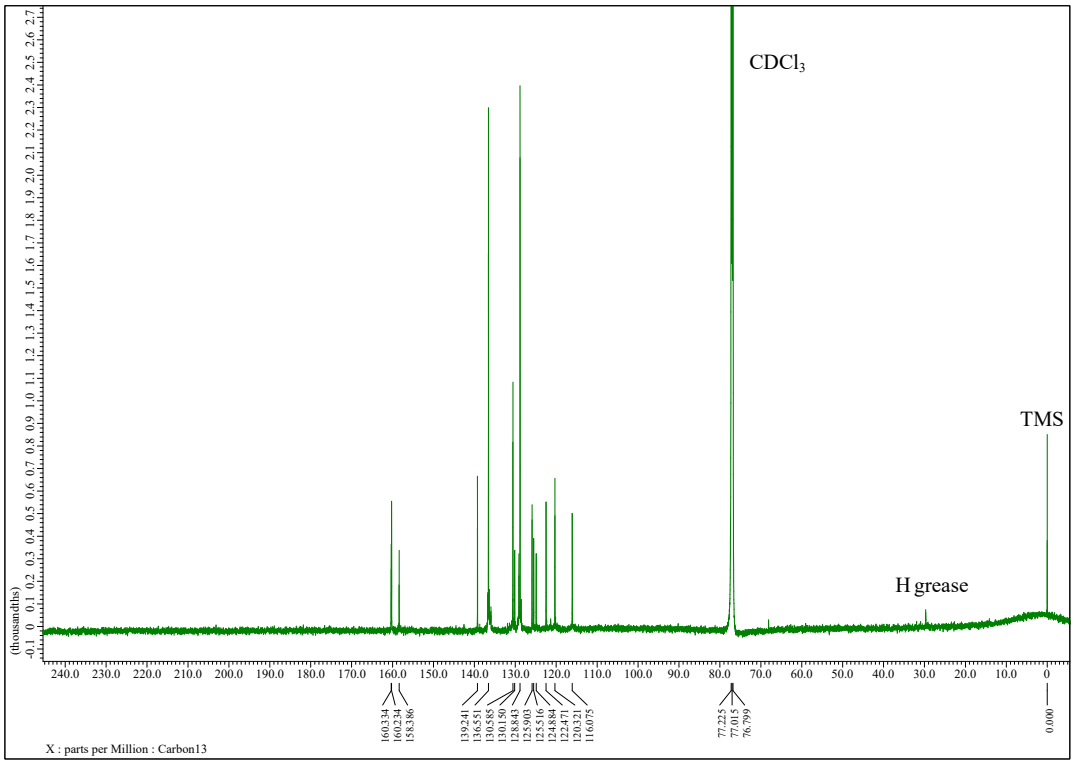

Chart S20. ^{13}C{^{1}H} NMR spectrum of **TPhNCBr** in $CDCl_3$ at 150 MHz.

TMS

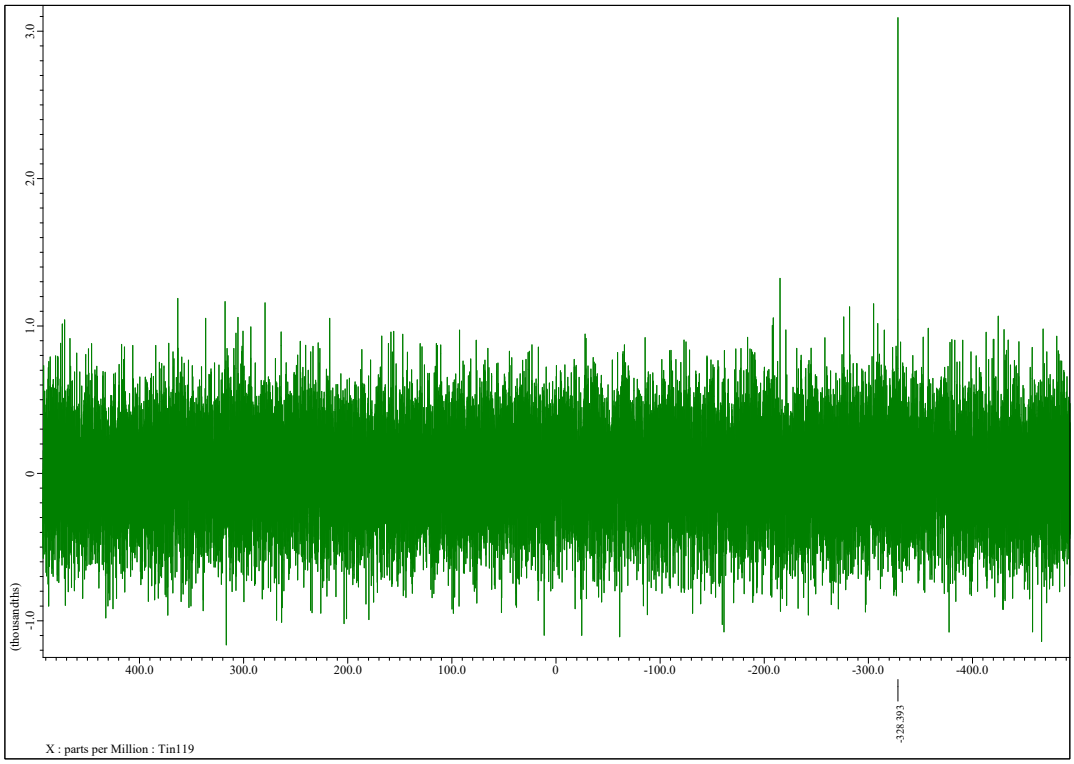

Chart S21. ^{119}Sn NMR spectrum of **TPhNCBr** in $CDCl_3$ at 149 MHz.

Synthesis of Polymers

Synthesis of **P-TPh**

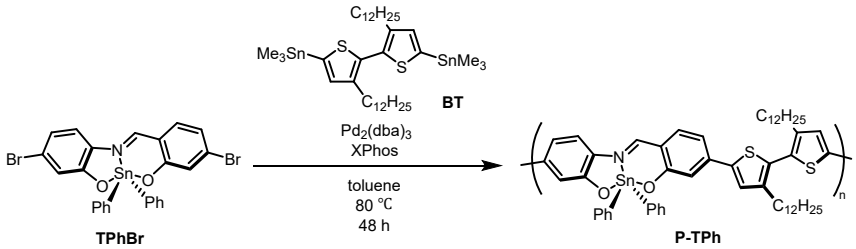

In a Schlenk tube, **TPhBr** (0.0700 g, 0.109 mmol, 1 equiv.), 5,5′-bis(trimethylstannyl)-3,3′-didodecyl-2,2′-bithiophene (**BT**) (0.0904 g, 0.109 mmol, 1 equiv.), $Pd_2(dba)_3$ (0.0030 g, 0.0033 mmol, 0.03 equiv.), XPhos (0.0031 g, 0.0065 mmol, 0.06 equiv.) were added. Then, under N_2, 2.00 mL of toluene was added and stirred at 80 °C for 24 h. After adding a small amount of $CHCl_3$, the reaction mixture was filtered with cotton and poured into a large amount of acetonitrile to collect the polymer by filtration. After the polymer was washed with acetone, it was extracted with $CHCl_3$ using a Soxhlet extractor to afford **P-TPh** as a green solid (0.0104 g, 10%).

Characterization:

$M_n = 4.1 \times 10^3$, PDI = 1.43, ^{1}H NMR ($CDCl_3$, 400 MHz) δ 8.62, 7.92, 7.62−6.99 (m), 6.63, 3.64, 2.57−2.47 (m), 1.47, 1.39−0.97 (m), 1.24−0.73 (m) ppm. $^{13}C\{^1H\}$ NMR ($CDCl_3$, 100 MHz) δ 77.3, 77.0, 76.7, 31.9, 29.7, 29.5, 29.4, 22.7, 14.1 ppm. The other $^{13}C\{^1H\}$ signals were not detected, probably because of broadening peaks in a polymer. ^{119}Sn NMR signal was not detected, probably because of low solubility and broadening peaks in a polymer. The peaks in an aromatic area are unclear due to broadened peaks.

GPC chart:

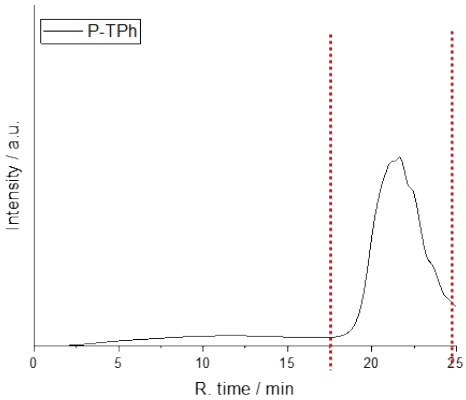

Chart S22. Gel permeation chromatography (GPC) profiles of **P-TPhCN**. Molecular weights were evaluated with chloroform as an eluent (1.0 mL/min) at 40 °C.

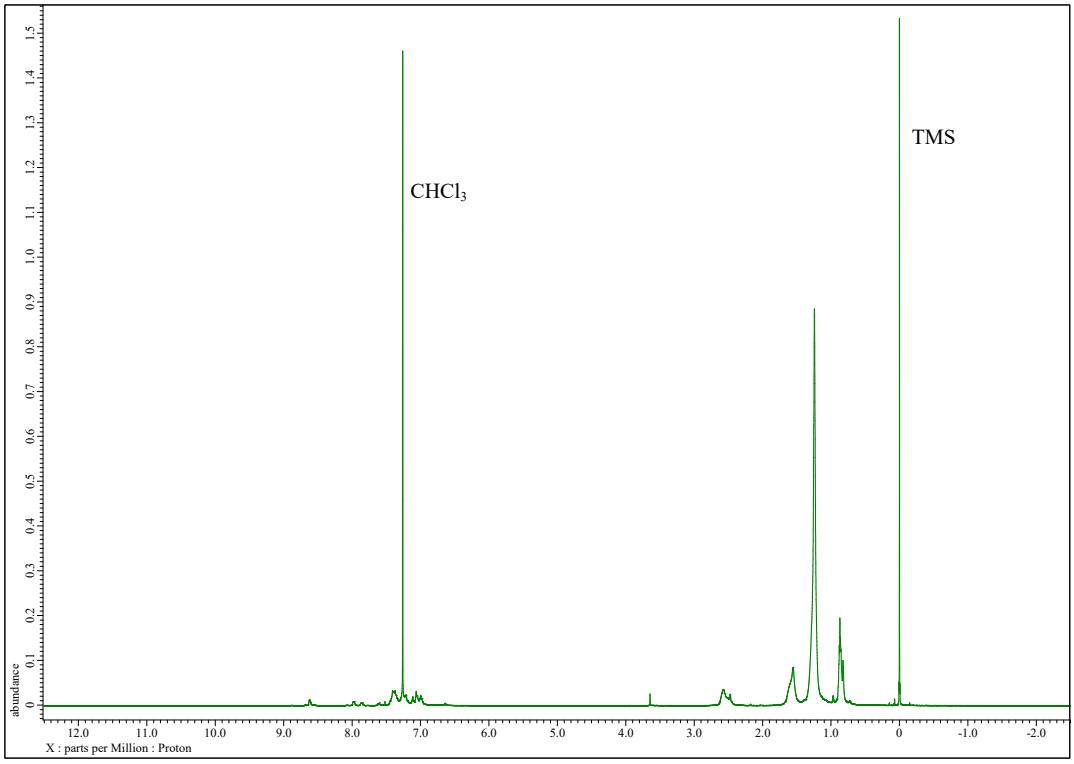

Chart 23. ^{1}H NMR spectrum of **P-TPh** in $CDCl_3$ at 400 MHz.

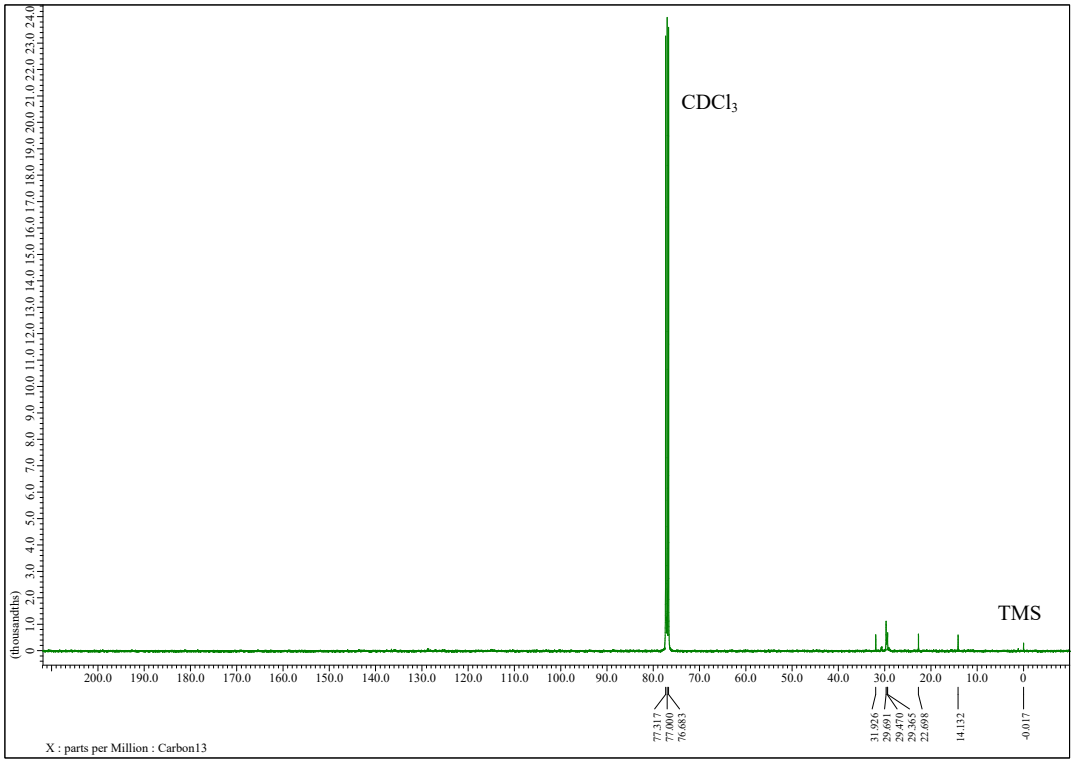

Chart 24. ^{13}C{^{1}H} NMR spectrum of **P-TPh** in $CDCl_3$ at 100 MHz.

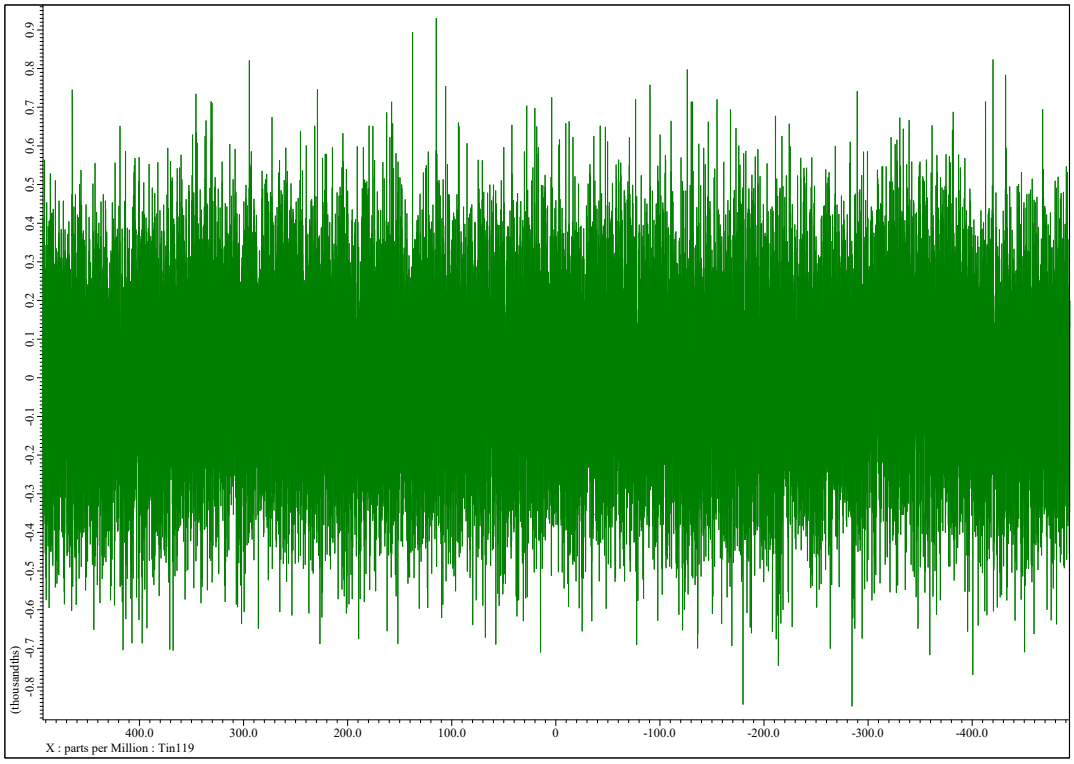

Chart S25. ^{119}Sn NMR spectrum of **P-TPh** in $CDCl_3$ at 149 MHz.

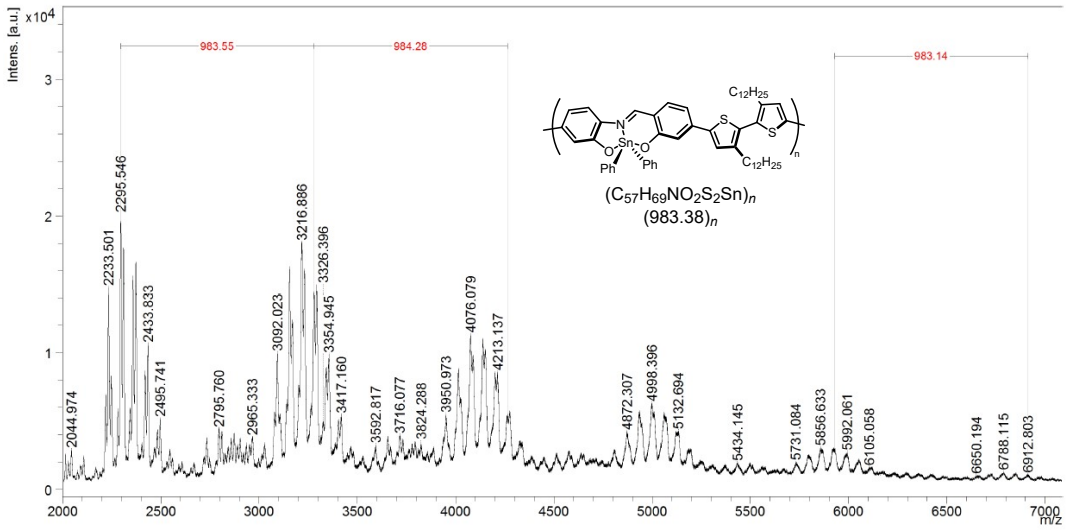

Chart S26. MALDI-TOF MS spectrum of **P-TPh**.

Synthesis of **P-TPhCN**

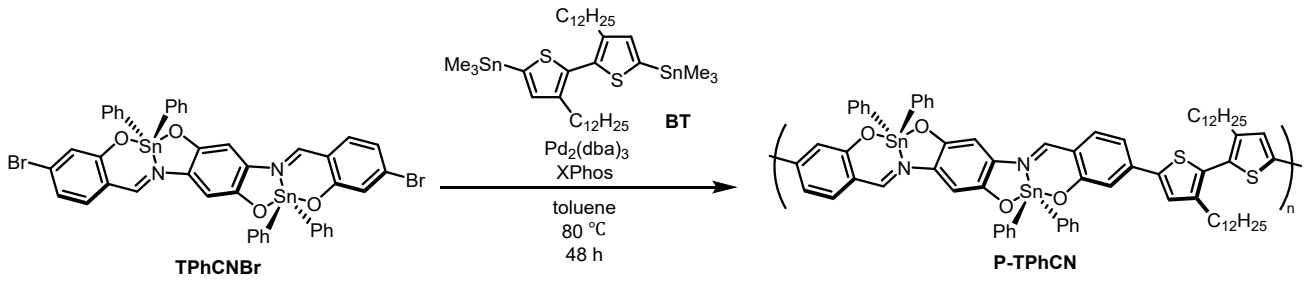

In a Schlenk tube, **TPhCNBr** (0.110 g, 0.105 mmol, 1 equiv.), 5,5′-bis(trimethylstannyl)-3,3′-didodecyl-2,2′-bithiophene (**BT**) (0.0870 g, 0.105 mmol, 1 equiv.), $Pd_2(dba)_3$ (0.0029 g, 0.0031 mmol, 0.03 equiv.), XPhos (0.0030 g, 0.0063 mmol, 0.06 equiv.) were added. Then, under N_2, 2.00 mL of toluene was added and stirred at 80 °C for 24 h. After adding a small amount of $CHCl_3$, the reaction mixture was filtered with cotton and poured into a large amount of acetonitrile to collect the polymer by filtration. After the polymer was washed with acetone, it was extracted with $CHCl_3$ using a Soxhlet extractor to afford **P-TPhCN** as a green solid (0.040 g, 28%).

Characterization:

M_n = 1.8 × 10^4, PDI = 5943, ^{1}H NMR ($CDCl_3$, 400 MHz) δ 8.63, 7.89, 7.40, 2.62, 1.26, 0.87 ppm. $^{13}C\{^1H\}$ NMR ($CDCl_3$, 150 MHz) δ 169.5, 159.6, 151.0, 143.9, 142.6, 142.0, 140.1, 136.6, 136.0, 133.0, 130.7, 130.3, 128.7, 127.2, 117.9, 117.4, 115.3, 103.1, 31.9, 30.8, 29.7, 29.4, 22.7, 14.15, 1.0 ppm. ^{119}Sn NMR ($CDCl_3$, 149 MHz) δ −324.7 ppm. The peaks in an aromatic area are unclear due to broadened peaks.

GPC chart:

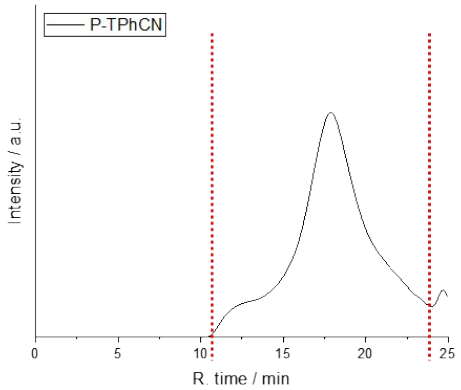

Chart S27. Gel permeation chromatography (GPC) profiles of **P-TPhCN**. Molecular weights were evaluated with chloroform as an eluent (1.0 mL/min) at 40 °C.

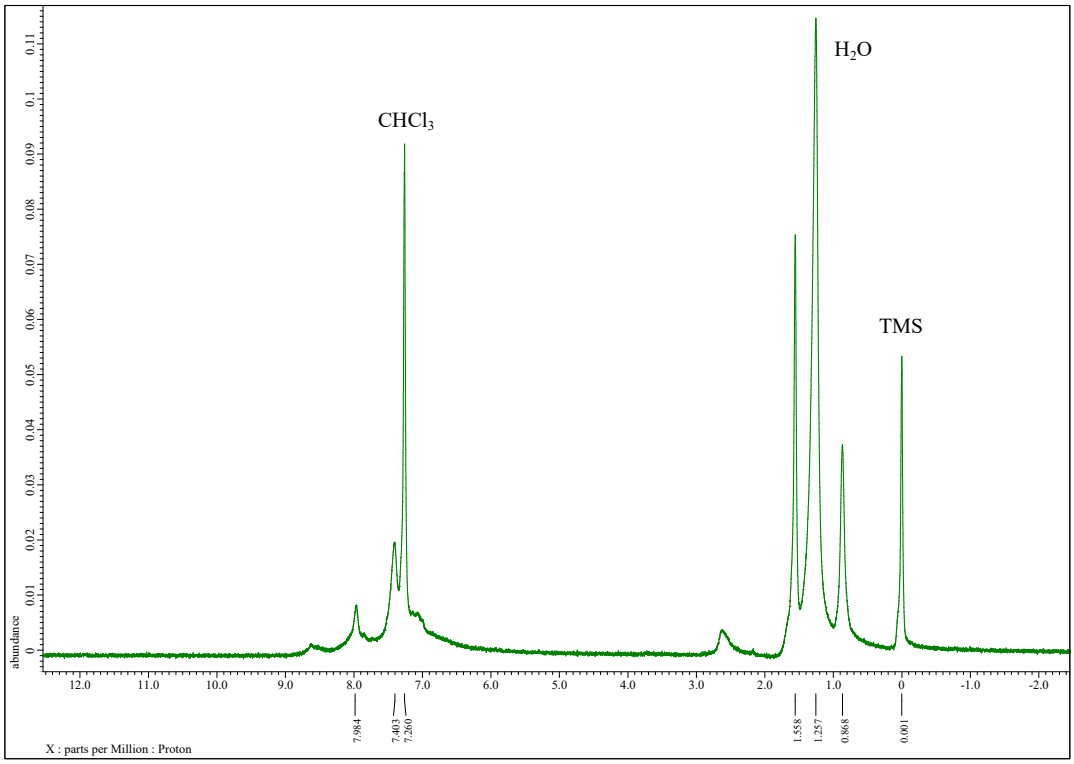

Chart S28. ^{1}H NMR spectrum of **P-TPhCN** in $CDCl_3$ at 400 MHz.

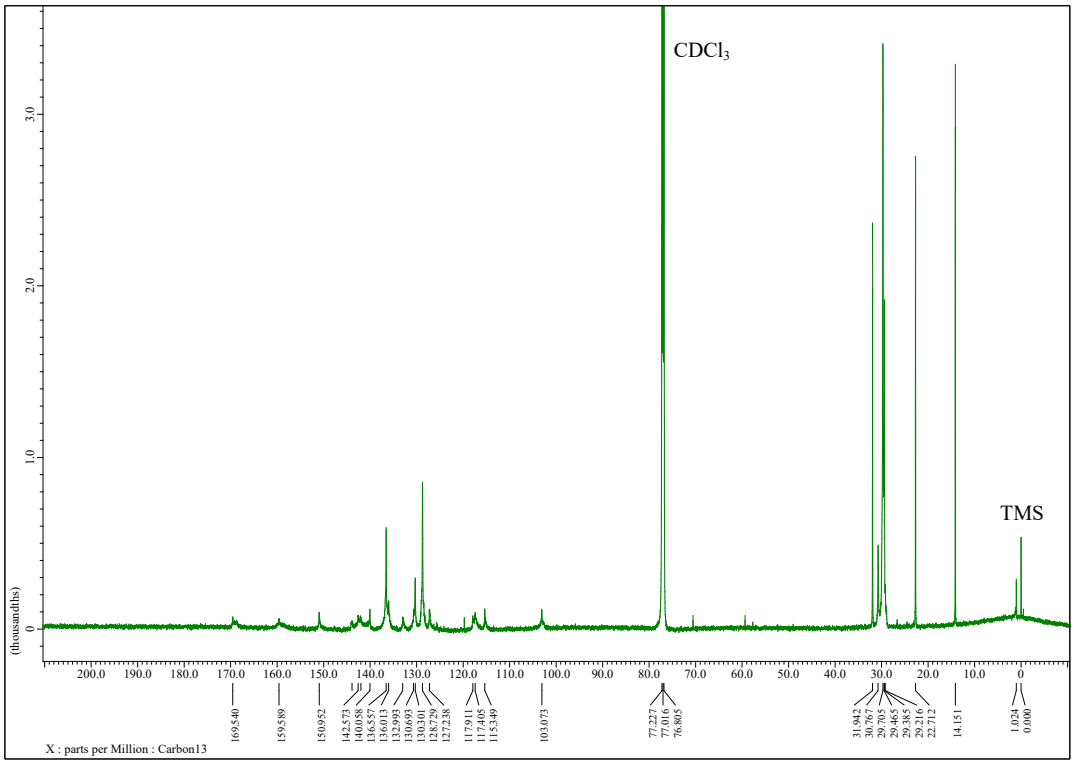

Chart S29. ^{13}C{^{1}H} NMR spectrum of **P-TPhCN** in $CDCl_3$ at 150 MHz.

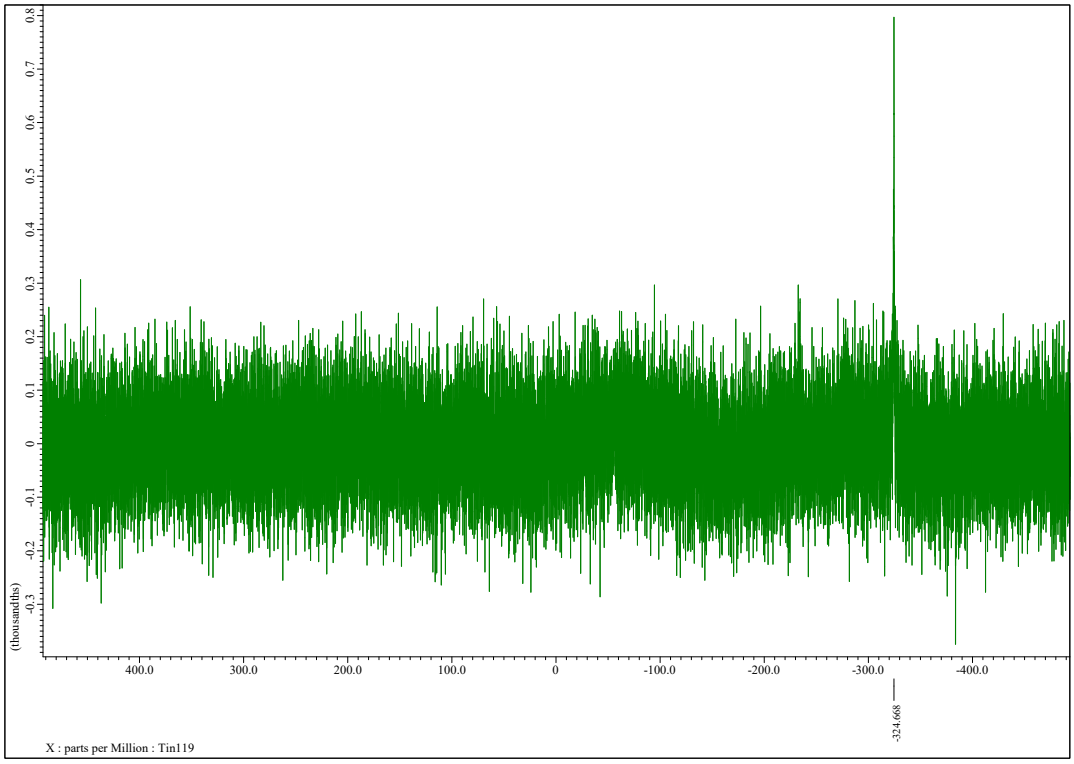

Chart S30. ^{119}Sn NMR spectrum of **P-TPhCN** in $CDCl_3$ at 149 MHz.

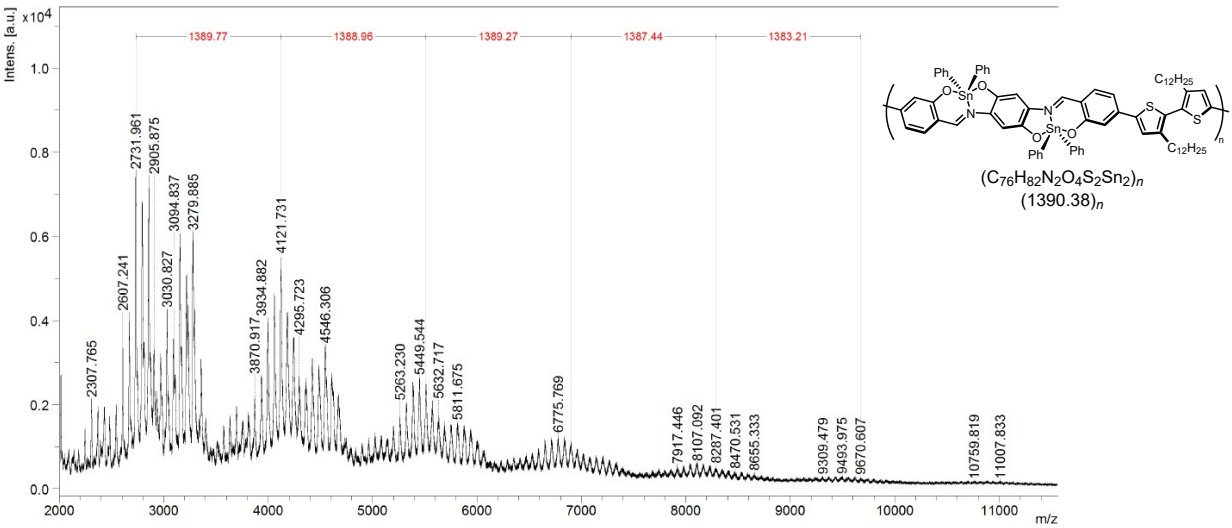

Chart S31. MALDI-TOF MS spectrum of **P-TPhCN**.

Synthesis of **P-TPhNC**

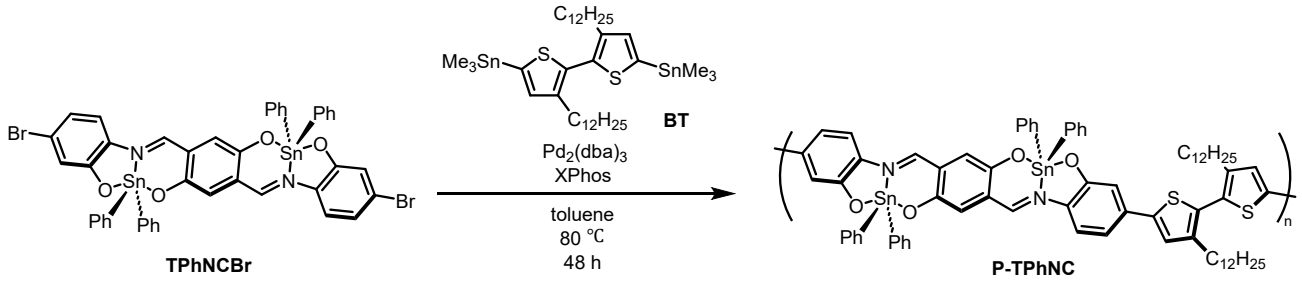

In a Schlenk tube, **TPhNCBr** (0.110 g, 0.105 mmol, 1 equiv.), 5,5′-bis(trimethylstannyl)-3,3′-didodecyl-2,2′-bithiophene (**BT**) (0.0870 g, 0.105 mmol, 1 equiv.), $Pd_2(dba)_3$ (0.0028 g, 0.0031 mmol, 0.03 equiv.), XPhos (0.0037 g, 0.0078 mmol, 0.07 equiv.) were added. Then, under N_2, 2.00 mL of toluene was added and stirred at 80 °C for 24 h. After adding a small amount of $CHCl_3$, the crude product was filtered with cotton and poured into a large amount of acetonitrile to collect the polymer by filtration. After the polymer was washed with acetone, it was extracted with $CHCl_3$ using a Soxhlet extractor to afford **P-TPhNC** as a purple-black solid (0.039 g, 27%).

Characterization:

$M_n = 1.3 \times 10^4$, $M_w = 3.9 \times 10^4$, $M_w/M_n = 3.0$. ^{1}H NMR ($CDCl_3$, 400 MHz) δ 8.70, 7.95, 7.40, 3.64, 2.48, 1.25, 0.86 ppm. $^{13}C\{^1H\}$ NMR ($CDCl_3$, 150 MHz) δ 158.3, 143.5, 142.8, 136.4, 128.8, 125.5, 115.4, 31.9, 30.7, 29.7, 29.5, 29.4, 22.7, 14.2, 1.0 ppm. The peaks in an aromatic area are unclear due to broadened peaks. ^{119}Sn NMR signal was not detected, probably because of broadening peaks in a polymer.

GPC chart:

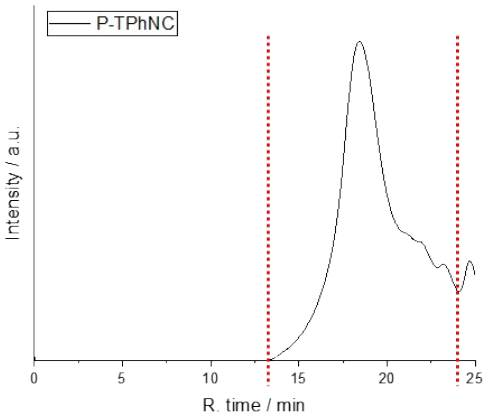

Chart S32. Gel permeation chromatography (GPC) profiles of **P-TPhNC**. Molecular weights were evaluated with chloroform as an eluent (1.0 mL/min) at 40 °C.

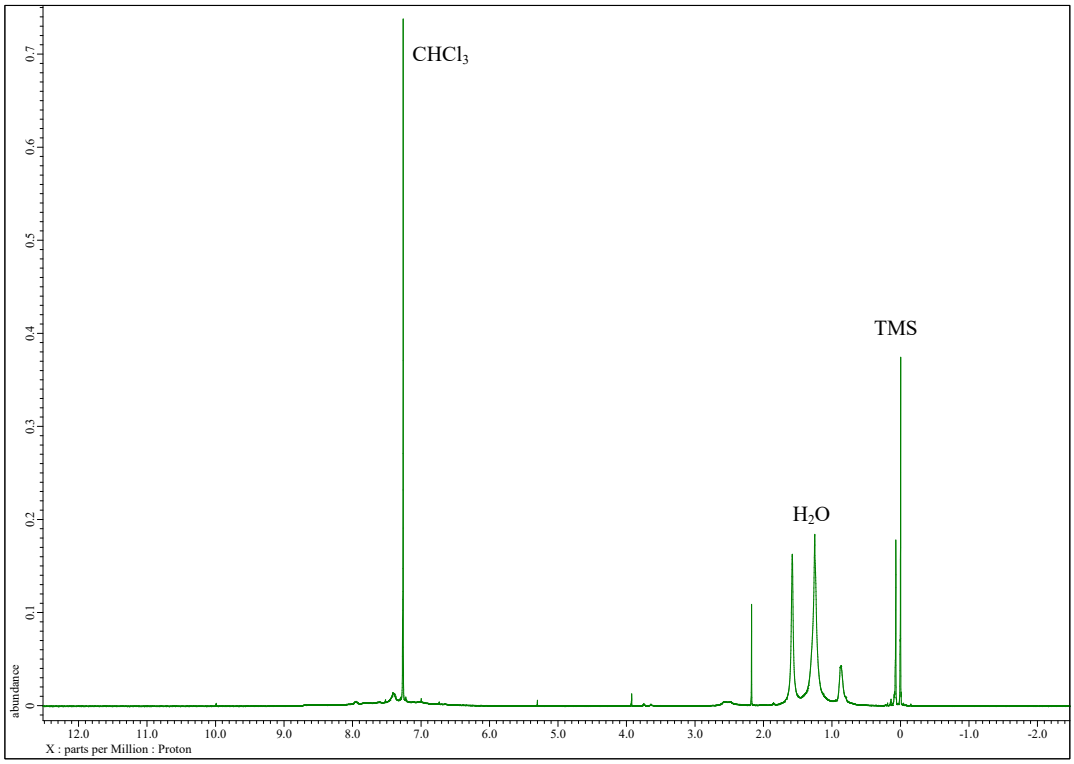

Chart S33. ^{1}H NMR spectrum of **P-TPhNC** in $CDCl_3$ at 400 MHz.

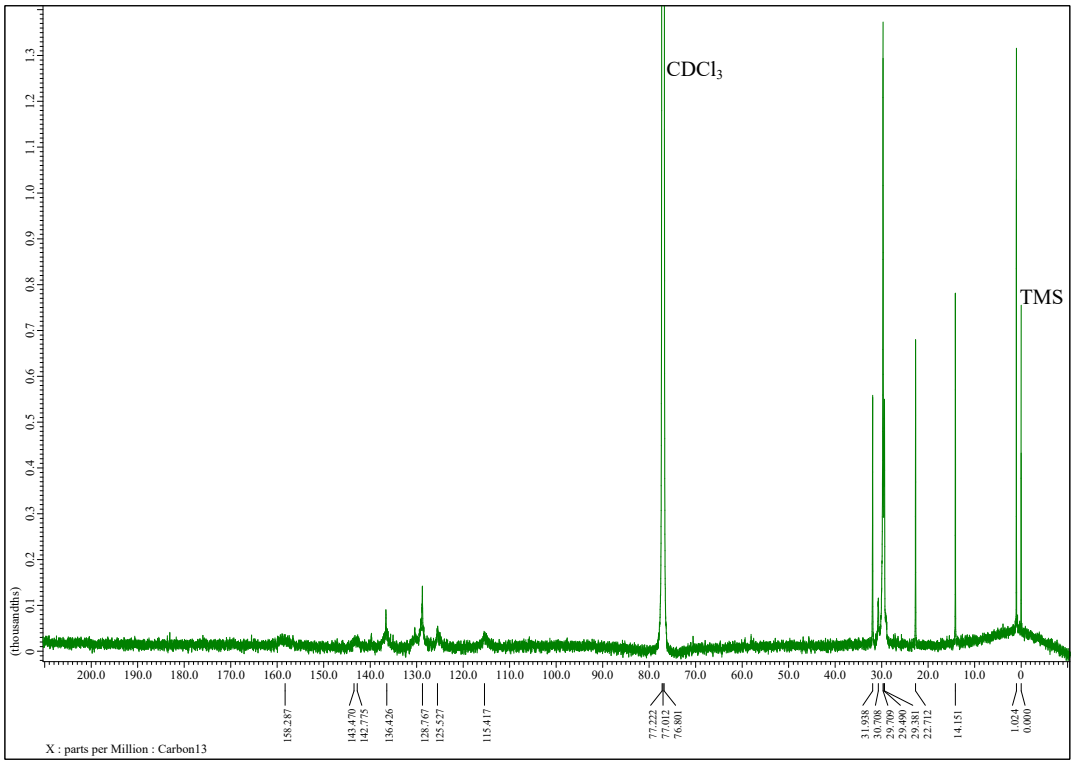

Chart S34. ^{13}C{^{1}H} NMR spectrum of **P-TPhNC** in $CDCl_3$ at 150 MHz.

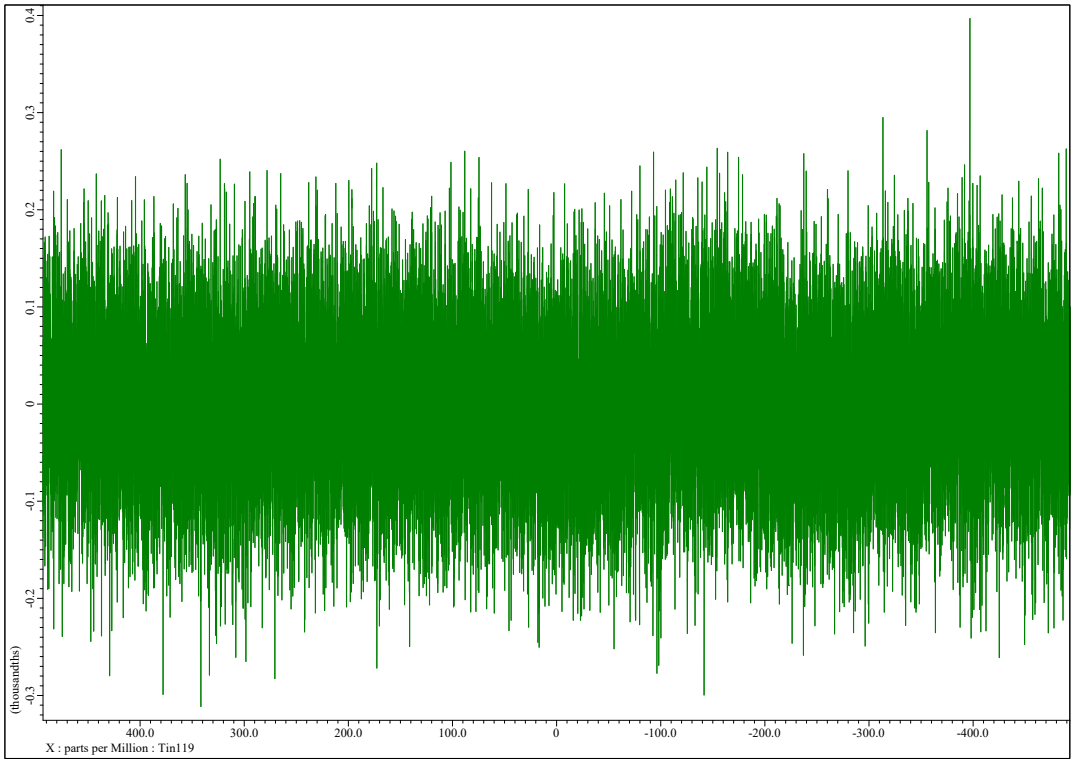

Chart S35. ^{119}Sn NMR spectrum of **P-TPhNC** in $CDCl_3$ at 149 MHz.

Stabilities of TPh derivatives

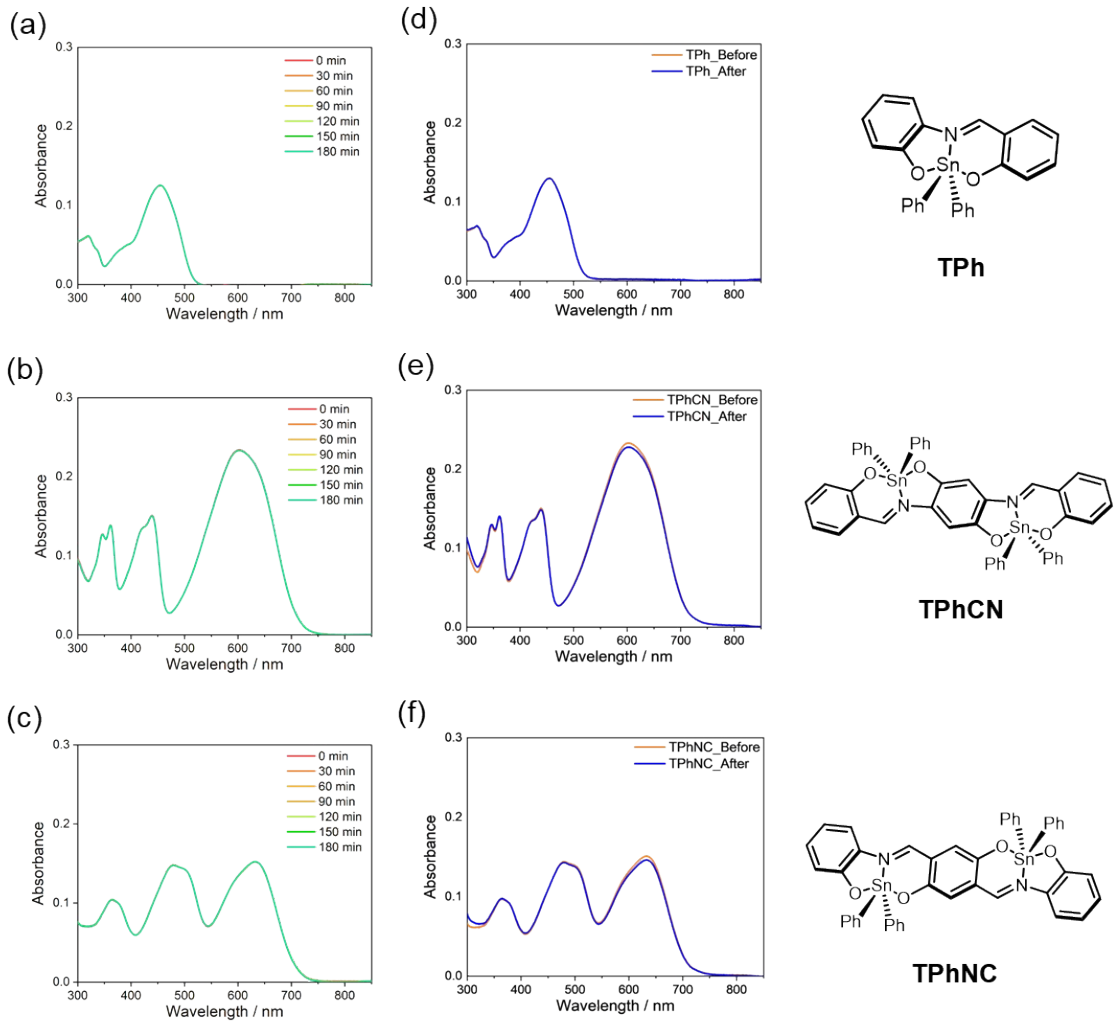

Figure S1. Time-dependent UV–vis absorption spectra of (a) **TPh**, (b) **TPhCN**, and (c) **TPhNC** (1.0×10^{-5} M in toluene). UV–vis absorption spectra before and after photo-irradiation of (d) **TPh**, (e) **TPhCN**, and (f) **TPhNC** (1.0×10^{-5} M in toluene) with trans-illuminator (365 nm, 6500 μWcm^{-2}, 60 s).

Stabilities of polymers

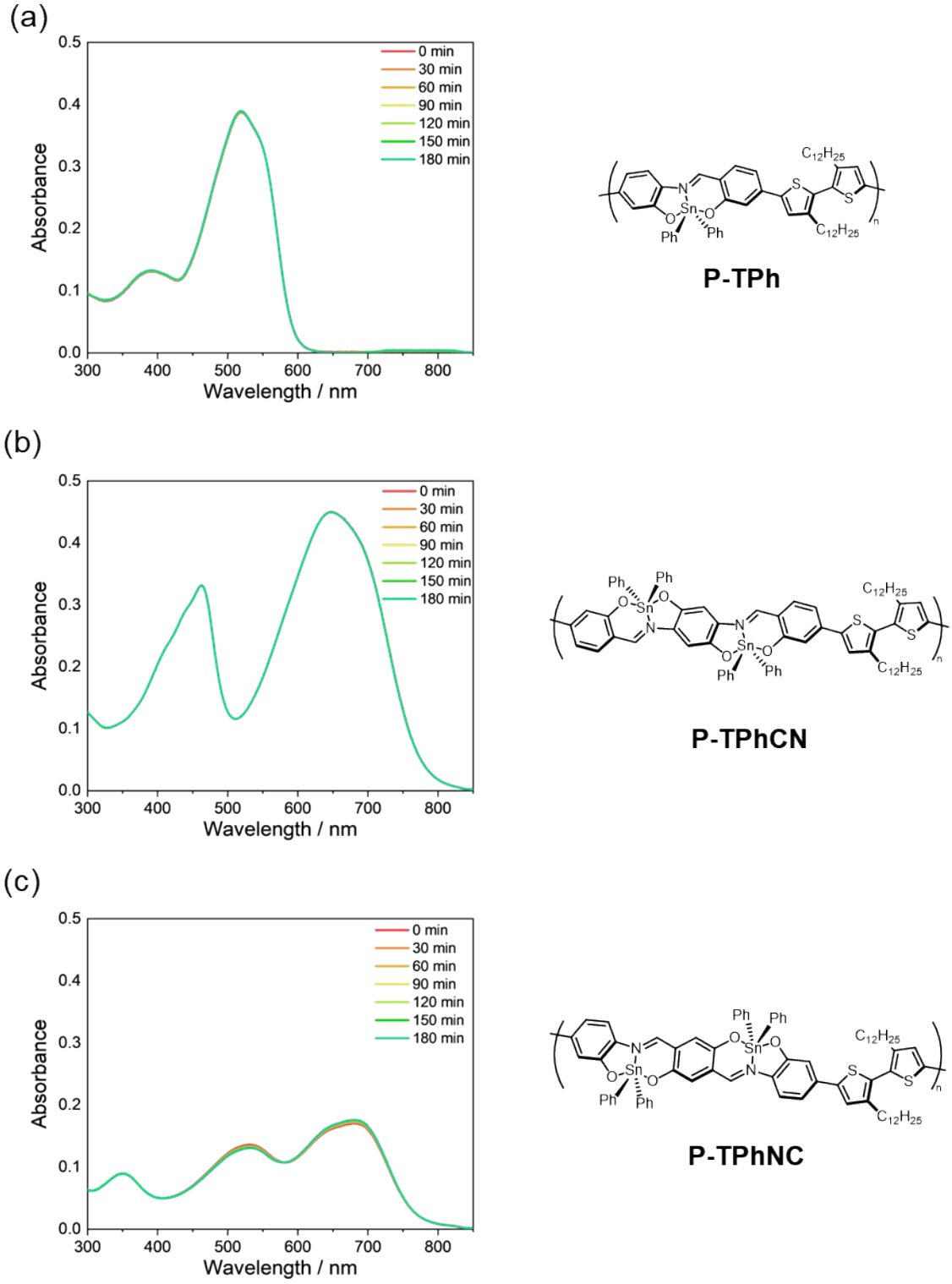

Figure S2. Time-dependent UV–vis absorption spectra of (a) **P-TPh**, (b) **P-TPhCN**, and (c) **P-TPhNC** (ca. 1.0×10^{-5} M per repeating unit in $CHCl_3$).

Single crystal X-ray structure analysis of TPhCN

Intensity data were collected on a Rigaku Saturn 724+ with MicroMax-007HF CCD diffractometer with Varimax Mo optics using graphite-monochromated MoKα radiation. The structure s were solved and refined by full-matrix least-squares procedures based on F^2 (SHELXL-2018/3).[7]

Table S1. Crystallographic data of **TPhCN**

Empirical formula	**C44 H32 N2 O4 Sn2**	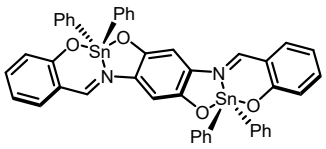
Formula weight	890.09	
Temperature (K)	143(2)	
Wavelength (Å)	0.71075	CCDC # 2373875
Crystal system, space group	Monoclinic, $P\ 2_1/n$	
Unit cell dimensions (Å)	a = 8.233(5)	
	b = 8.661(5)	
	c = 25.432(16)	
Unit cell dimensions (°)	α = 90	
	β = 96.086(8)	
	γ = 90	
Volume (Å^3)	1803.2(19)	
Z, calculated density (g cm^{-3})	2, 1.639	
Absorption coefficient	1.432	
F(000)	884.0	
Crystal size (mm)	0.09×0.06×0.03	
θ range for data collection (°)	3.2-27.5	
Limiting indices	$-8 \le h \le 10$, $-11 \le k \le 11$, $-32 \le l \le 32$	
Reflections collected (unique)	13811/4078, [R(int)=0.1233]	
Completeness to theta	0.997	
Max. and min. transmission	1.000, 0.691	
Goodness-of-fit on F^2	1.300	
Final R indices [$I > 2\sigma(I)$][a]	R_1 = 0.1216, wR_2 = 0.1581	
R indices (all data)	R_1 = 0.1589, wR_2 = 0.1729	

[a] $R_1 = \Sigma(|F_0|-|F_c|)/\Sigma|F_0|$. w$R2 = [\Sigma w(F^2_0-F^2_c)2/\Sigma w(F^2_0)^2]^{1/2}$. $w = 1/[\sigma^2(F^2_0)+[(ap)^2+bp]]$, where $p = [\max(F^2_0,0)+2F^2_c]/3$.

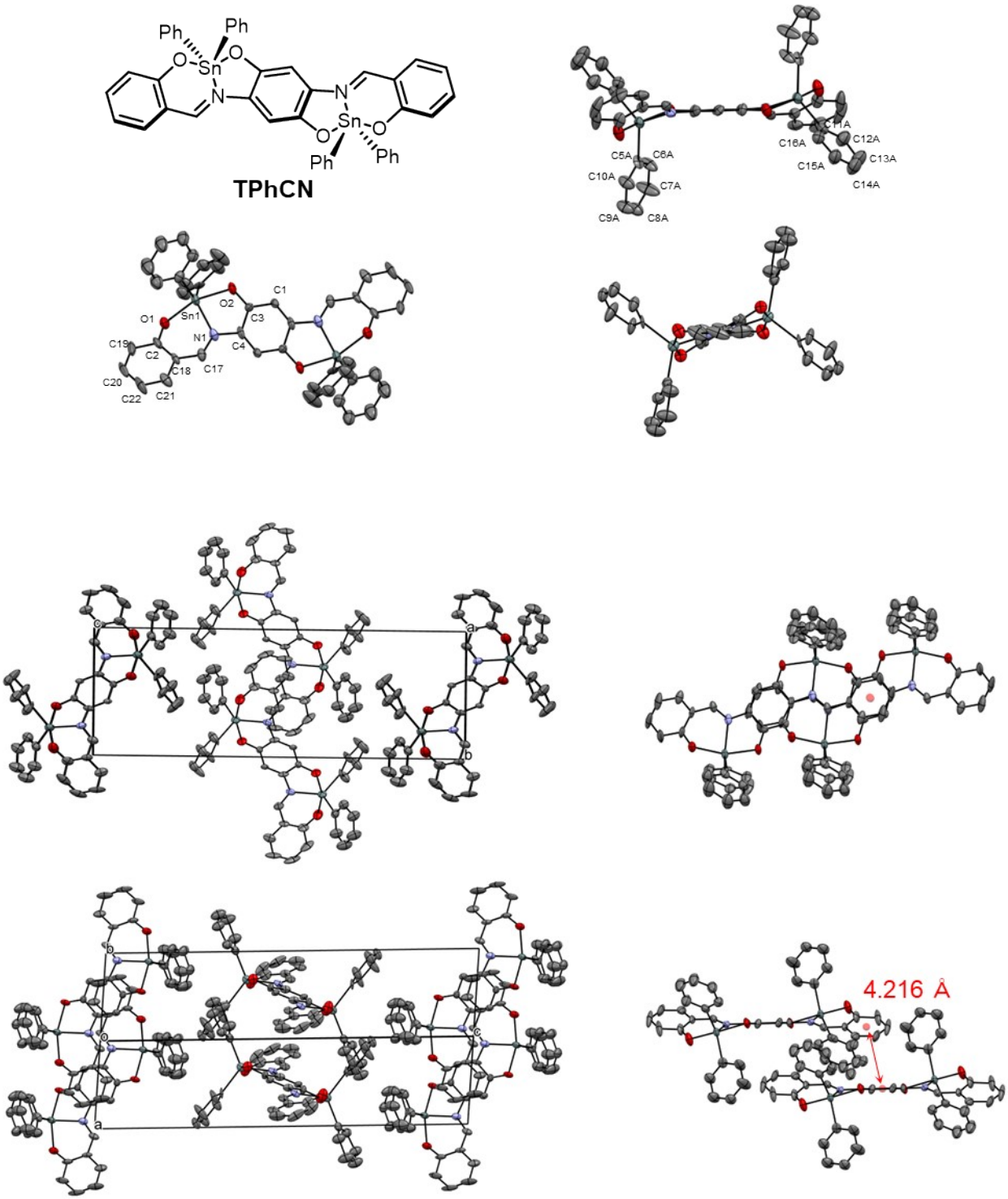

Figure S3. ORTEP drawings of **TPhCN**. Thermal ellipsoids are scaled to the 50% probability level. Hydrogen atoms are omitted for clarity.

Single crystal X-ray structure analysis of TPhNC

Intensity data were collected on a Rigaku Saturn 724+ with MicroMax-007HF CCD diffractometer with Varimax Mo optics using graphite-monochromated MoKα radiation. The structures were solved and refined by full-matrix least-squares procedures based on F^2 (SHELXL-2018/3).[7]

Table S2. Crystallographic data of **TPhNC**

Empirical formula	**C44 H32 N2 O4 Sn2**	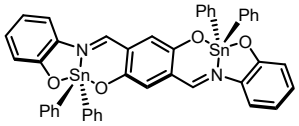
Formula weight	890.09	
Temperature (K)	143(2)	
Wavelength (Å)	0.71075	CCDC # 2373876
Crystal system, space group	Triclinic, *P* -1	
Unit cell dimensions (Å)	a = 9.383(8)	
	b = 12.3335(10)	
	c = 16.264(14)	
Unit cell dimensions (°)	α = 80.34(2)	
	β = 84.76(3)	
	γ = 82.51(3)	
Volume (Å^3)	1835(2)	
Z, calculated density (g cm^{-3})	2, 1.611	
Absorption coefficient	1.408	
F(000)	884	
Crystal size (mm)	0.11×0.05×0.03	
θ range for data collection (°)	3.1-27.5	
Limiting indices	$-12 \le h \le 11$, $-15 \le k \le 15$, $-20 \le l \le 20$	
Reflections collected (unique)	14361/7845, [R(int)=0.0810]	
Completeness to theta	0.974	
Max. and min. transmission	1.000, 0.657	
Goodness-of-fit on F^2	1.083	
Final R indices [$I > 2\sigma(I)$][a]	R_1 = 0.0887, wR_2 = 0.1647	
R indices (all data)	R_1 = 0.1365, wR_2 = 0.1981	

[a] $R_1 = \Sigma(|F_0|-|F_c|)/\Sigma|F_0|$. w$R2 = [\Sigma w(F^2_0-F^2_c)2/\Sigma w(F^2_0)^2]^{1/2}$. $w = 1/[\sigma^2(F^2_0)+[(ap)^2+bp]]$, where $p = [\max(F^2_0,0)+2F^2_c]/3$.

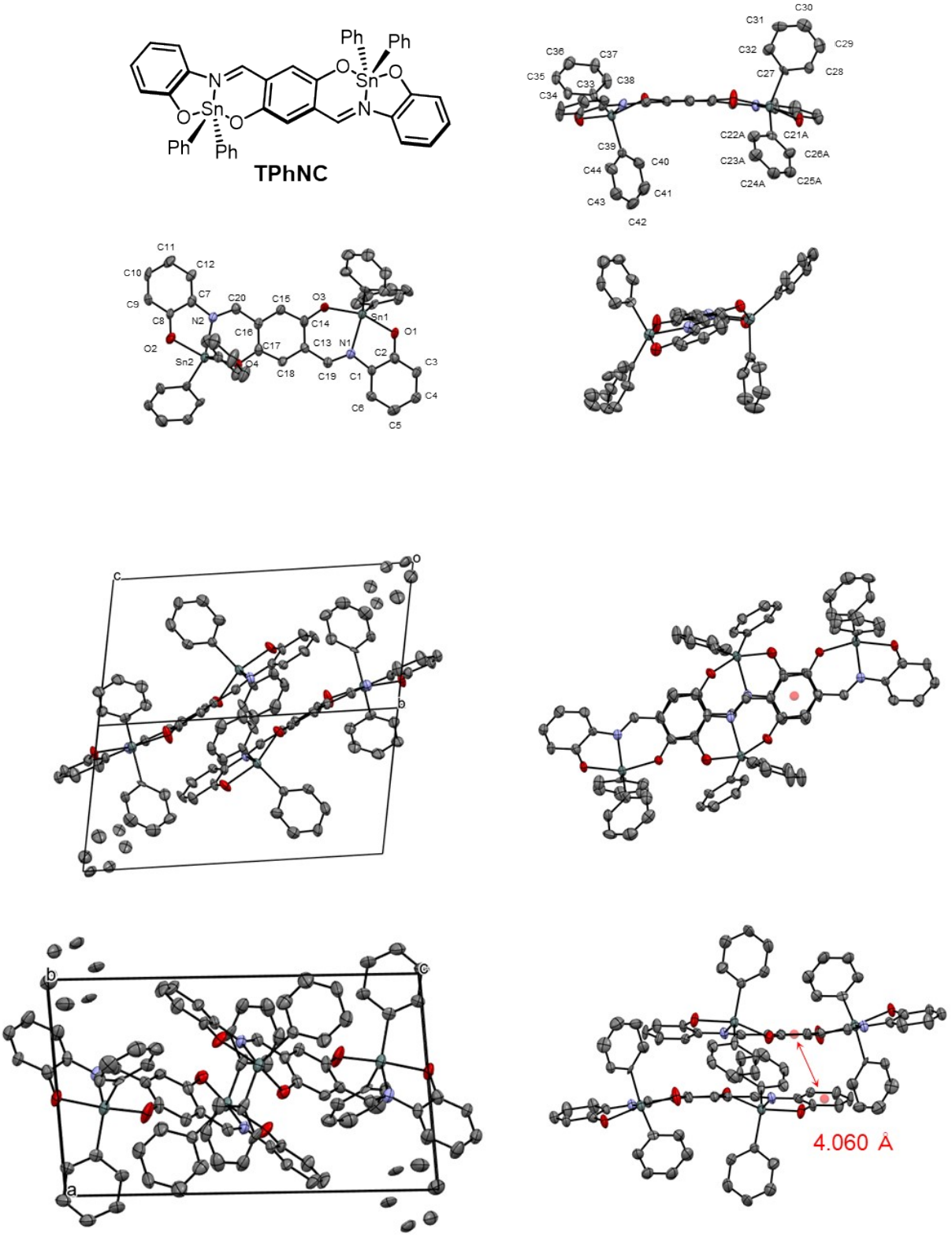

Figure S4. ORTEP drawings of **TPhNC**. Thermal ellipsoids are scaled to the 50% probability level. Hydrogen atoms are omitted for clarity.

Computational details for theoretical calculation in Azm, AzmOMe, and TPh

The Gaussian 16 program package[9] was used for computation. We optimized the structures of **Azm**, **AzmOMe**, and **TPh** in the ground S_0 states and calculated their orbitals. The DFT was applied to optimize the structures in the S_0 states at B3LYP/6-31G(d) for C, H, N, O and LanL2DZ for Sn. We calculated the energy of the S_0–S_1 transitions with optimized geometries in the S_0 states by time-dependent (TD)-DFT at B3LYP/6-31G(d) for C, H, N, O and LanL2DZ for Sn.

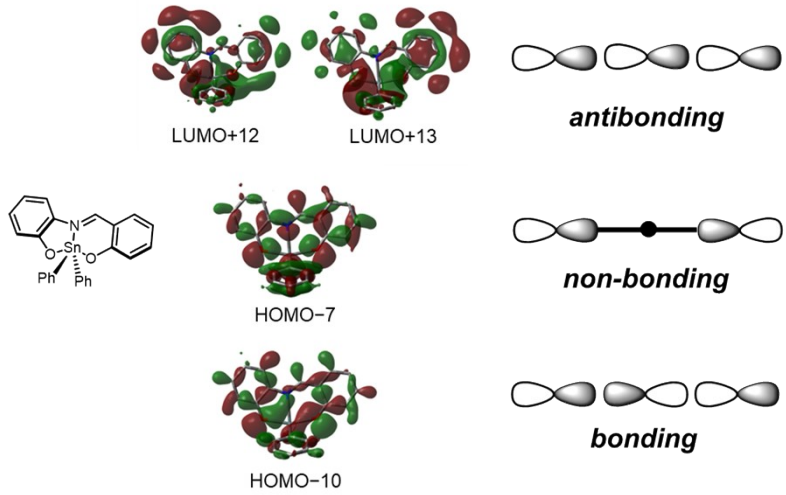

Figure S5. Bonding, non-bonding, and antibonding orbitals in the hypervalent O−Sn−O bond of **TPh** obtained with DFT and TD-DFT calculations at the TD-B3LYP/6-31G(d)//B3LYP/6-31G(d) level for C, H, N, and O and LanL2DZ for Br and Sn (isovalue = 0.02).

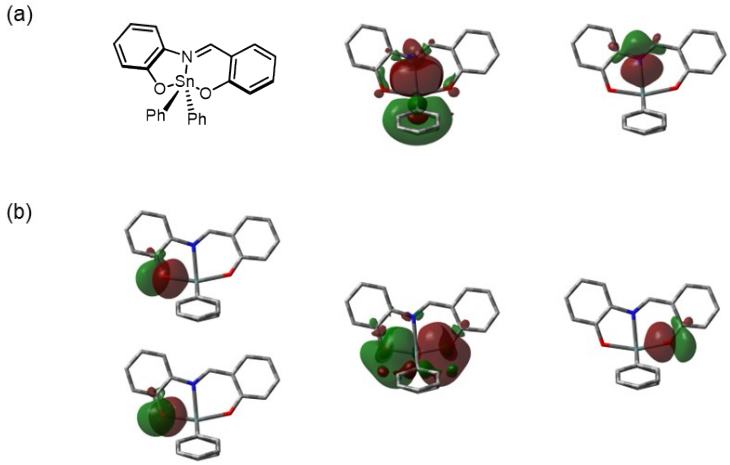

Figure S6. (a) NBO plots showing the donor–acceptor interaction between a vacant p(Sn) orbital with a filled p(N) orbital (isovalue = 0.02) in **TPh**. (b) The NBOs involved in the 3c-4e bond of **TPh**. The two oxygen lone pairs and the tin p orbital (isovalue = 0.02)

Table S3. Selected MOs of **TPh**[a]

LUMO+13	LUMO+12	LUMO+11	LUMO+10	LUMO+9
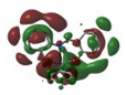	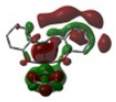	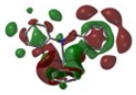	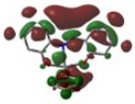	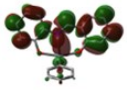
LUMO+8	LUMO+7	LUMO+6	LUMO+5	LUMO+4
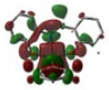	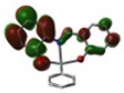	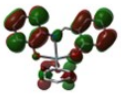	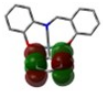	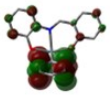
LUMO+3	LUMO+2	LUMO+1	LUMO	HOMO
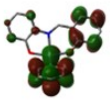	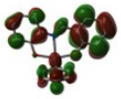	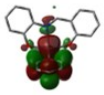	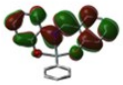	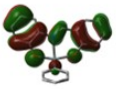
HOMO−1	HOMO−2	HOMO−3	HOMO−4	HOMO−5
		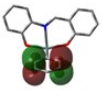	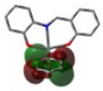	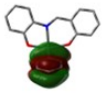
HOMO−6	HOMO−7	HOMO−8	HOMO−9	HOMO−10
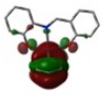	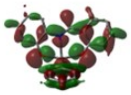		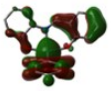	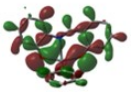
HOMO−11	HOMO−12	HOMO−13		
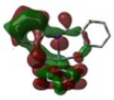	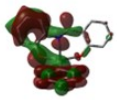	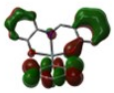	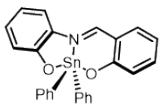	

[a]Obtained by DFT at TD-B3LYP/6-31G(d) and LanL2DZ level (isovalue = 0.02).

Table S4. Selected MOs and results of the transition of **Azm**[a]

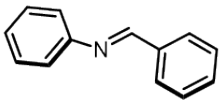

Azm

LUMO+2	LUMO	HOMO	HOMO−1	HOMO−2	HOMO−4
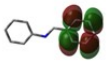		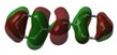			
−1.55 eV	**−5.90 eV**	**−6.72 eV**	**−6.82 eV**	**−6.97 eV**	**−7.57 eV**

Excited State	Excitation Energy / eV	Wavelength / nm	Oscillator Strength	Assignment (weight)
1	3.7460	330.98	0.2841	HOMO−4 -> LUMO (−0.13912) HOMO−2 -> LUMO (−0.21169) HOMO−1 -> LUMO (0.13157) HOMO -> LUMO (0.64024)
2	4.4930	275.95	0.0616	HOMO−2 -> LUMO (−0.12607) HOMO−1 -> LUMO (0.64818) HOMO -> LUMO (0.11071) HOMO -> LUMO+2 (0.20330)

[a]Obtained by DFT at TD-B3LYP/6-31G(d) and LanL2DZ level (isovalue = 0.02).

Table S5. Selected MOs and results of the transition of **AzmOMe**[a]

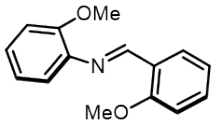

AzmOMe

LUMO	HOMO	HOMO−1	HOMO−2	HOMO−3	HOMO−4
			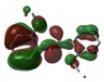		
−1.17 eV	**−5.22 eV**	**−5.94 eV**	**−6.12 eV**	**−6.52 eV**	**−7.19 eV**

Excited State	Excitation Energy / eV	Wavelength / nm	Oscillator Strength	Assignment (weight)
1	3.4095	363.64	0.2451	HOMO−3 -> LUMO (−0.15541) HOMO−1 -> LUMO (0.12030) HOMO -> LUMO (0.66400)
2	4.1581	298.17	0.1705	HOMO−4 -> LUMO (0.10860) HOMO−2 -> LUMO (0.46218) HOMO−1 -> LUMO (−0.46238) HOMO -> LUMO (0.17793)

[a]Obtained by DFT at TD-B3LYP/6-31G(d) and LanL2DZ level (isovalue = 0.02).

Table S6. Selected MOs and results of the transition of **TPh**[a]

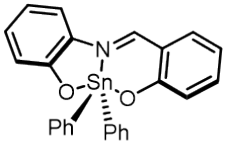

TPh

LUMO	HOMO	HOMO−1	HOMO−2	HOMO−3	HOMO−4
		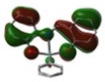			
−2.21 eV	**−5.41 eV**	**−6.07 eV**	**−6.56 eV**	**−6.59 eV**	**−6.61 eV**

Excited State	Excitation Energy / eV	Wavelength / nm	Oscillator Strength	Assignment (weight)
1	2.7812	445.80	0.2319	HOMO -> LUMO (0.69923)
2	3.3319	372.11	0.0474	HOMO−1 -> LUMO (0.69887)
3	3.8763	319.85	0.1939	HOMO−2 -> LUMO (0.68896)
4	3.8903	318.70	0.0032	HOMO−5 -> LUMO (0.69139) HOMO−3 -> LUMO (-0.12681)

[a]Obtained by DFT at TD-B3LYP/6-31G(d) and LanL2DZ level (isovalue = 0.02).

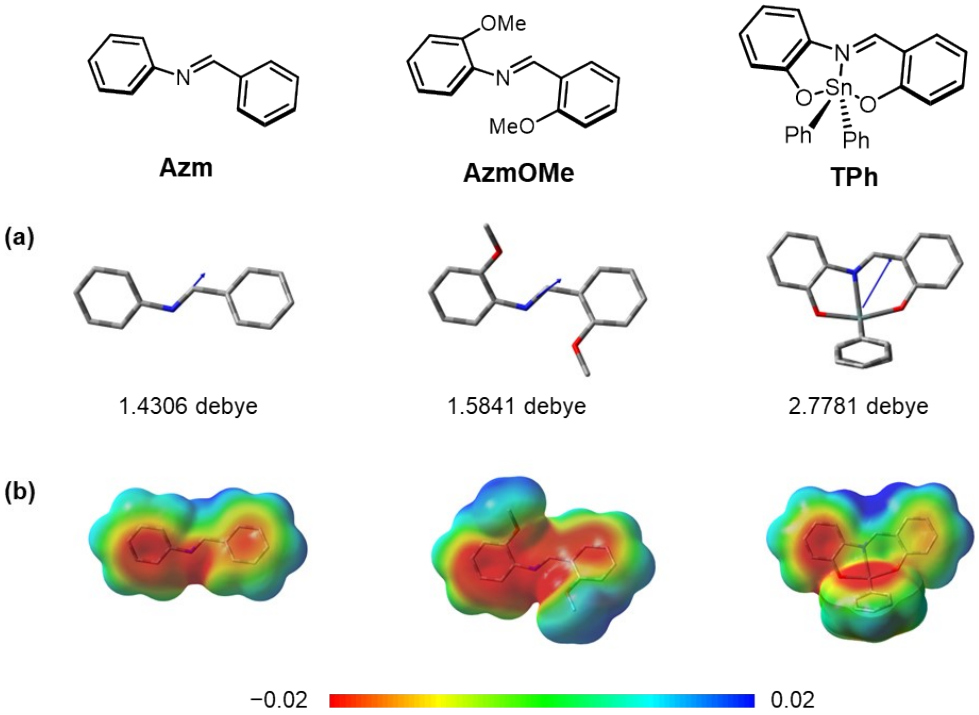

Figure S7. (a) Dipole moments and (b) molecular electrostatic potential (MEP) surfaces of **Azm**, **AzmOMe**, and **TPh** (TD-B3LYP/6-31G(d) for C, H, N, O, and LanL2DZ for Sn).

Computational details for theoretical calculation in TPh, TPhCN, and TPhNC

The Gaussian 16 program package[10] was used for computation. We optimized the structures of **TPh**, **TPhCN**, and **TPhNC** in the ground S_0 states and calculated their orbitals. The DFT was applied to optimize the structures in the S_0 states at B3LYP/6-31G(d) for C, H, N, O, and LanL2DZ for Sn. We calculated the energy of the S_0–S_1 transitions with optimized geometries in the S_0 states by time-dependent (TD)-DFT at B3LYP/6-31G(d) for C, H, N, O, and LanL2DZ for Sn.

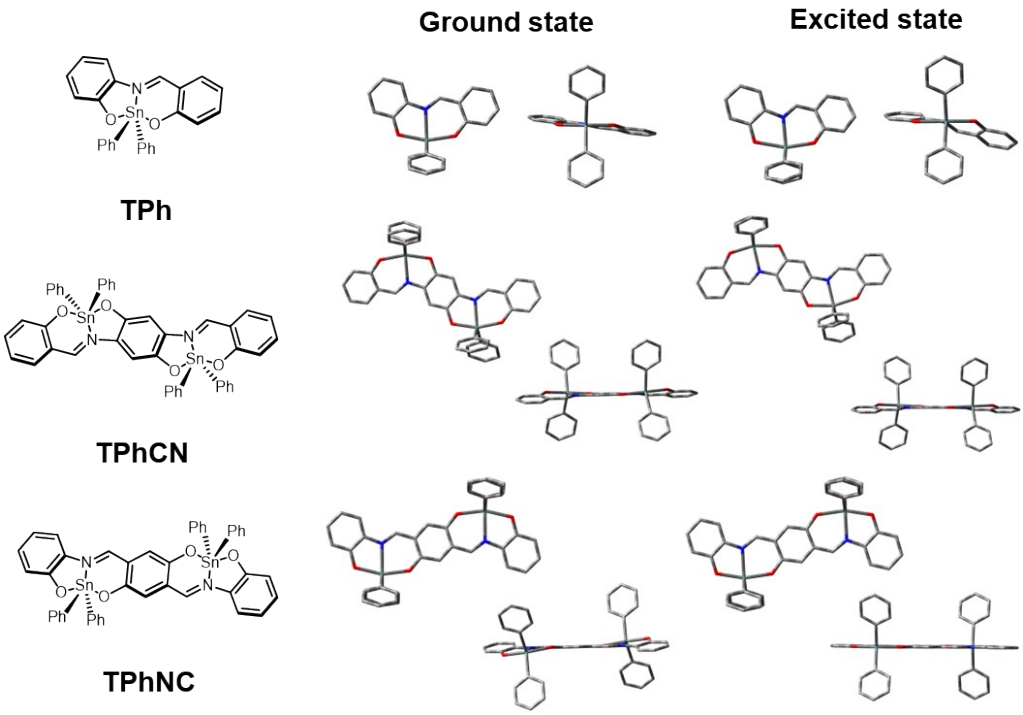

Figure S8. Optimized structures of TPh derivatives in the ground and excited state.

Table S7. Selected MOs and results of the transition of **TPhCN**[a]

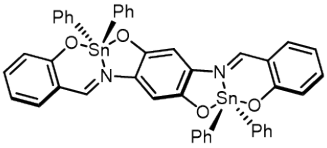

TPhCN

LUMO+1	LUMO	HOMO	HOMO−1	HOMO−2
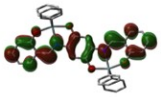	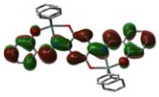	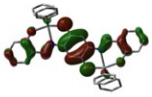	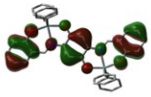	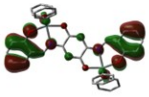
−1.82 eV	**−2.54 eV**	**−4.87 eV**	**−5.89 eV**	**−6.02 eV**

Excited State	Excitation Energy / eV	Wavelength / nm	Oscillator Strength	Assignment (weight)
1	2.0006	619.74	0.4496	HOMO -> LUMO (0.70313)
2	2.6375	470.08	0.0004	HOMO -> LUMO+1 (0.69719)
3	2.9109	425.92	0.3865	HOMO−1 -> LUMO (0.69755)
4	3.0597	405.22	0.0003	HOMO−2 -> LUMO (0.69534)
5	3.5021	354.03	0.3483	HOMO−3 -> LUMO (0.69455)

[a]Obtained by DFT at TD-B3LYP/6-31G(d) and LanL2DZ level (isovalue = 0.02).

Table S8. Selected MOs and results of the transition of **TPhNC**[a]

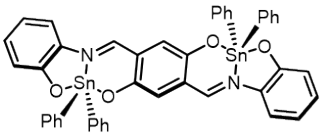

TPhNC

LUMO+1	LUMO	HOMO	HOMO−1	HOMO−2
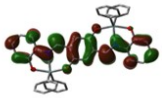	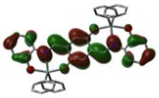	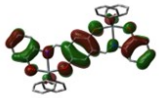	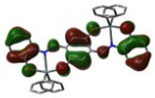	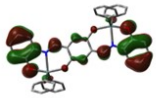
−1.50 eV	**−2.97 eV**	**−5.25 eV**	**−5.75 eV**	**−5.77 eV**

Excited State	Excitation Energy / eV	Wavelength / nm	Oscillator Strength	Assignment (weight)
1	1.9475	636.63	0.3843	HOMO -> LUMO (0.70147)
2	2.4053	515.46	0.3196	HOMO−1 -> LUMO (0.69933)
3	2.4497	506.11	0.0000	HOMO−2 -> LUMO (0.70085)
4	3.2129	385.90	0.0000	HOMO−12 -> LUMO (-0.16910) HOMO−10 -> LUMO (0.15137) HOMO -> LUMO+1 (0.65202)
5	3.2182	385.25	0.4931	HOMO−3 -> LUMO (0.69725)

[a]Obtained by DFT at TD-B3LYP/6-31G(d) and LanL2DZ level (isovalue = 0.02).

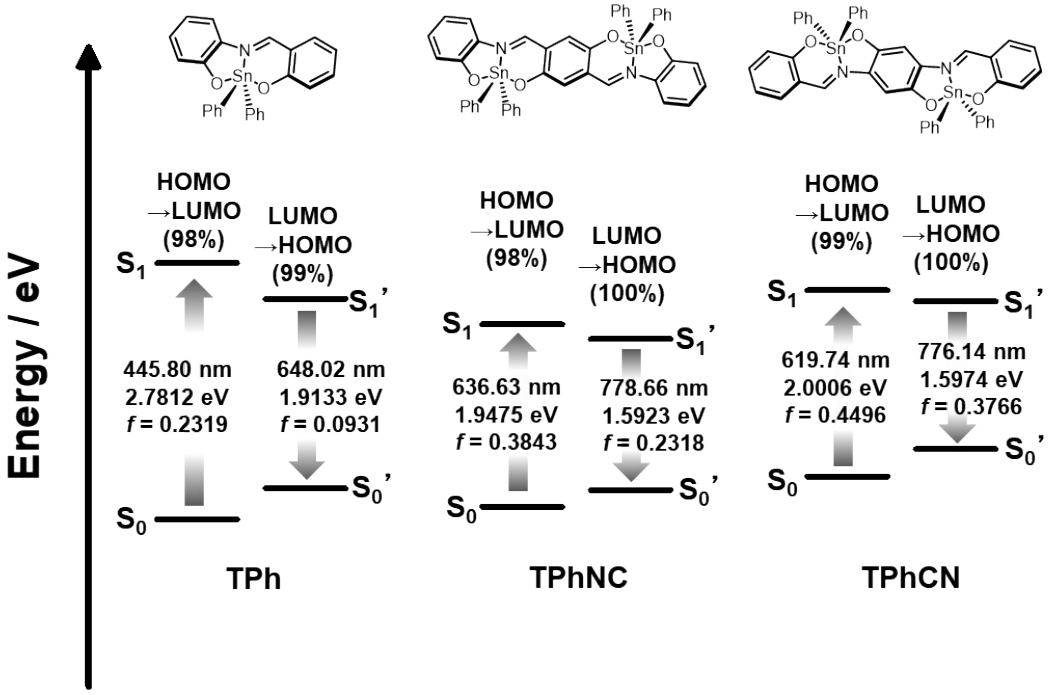

Figure S9. Energy diagrams, selected MOs, and oscillator strengths (*f*) of selected transition bands of **TPh**, **TPhCN**, and **TPhNC** obtained with DFT and TD-DFT calculations at TD-B3LYP/6-31G(d)//B3LYP/6-31G(d) level for C, H, N, O, and LanL2DZ for Sn (isovalue = 0.02).

Cyclic voltammograms

Experimental values of HOMO and LUMO energy levels (E_{HOMO} and $E_{LUMO,}$ respectively) were estimated by onset potential of oxidation (E_{onset}^{ox}) and reduction (E_{onset}^{red}) peaks by cyclic voltammetry, respectively, according to the literature with the equation of $E_{HOMO} = -4.8 - E_{onset}^{ox}$ /V and $E_{LUMO} = -4.8 - E_{onset}^{red}$ /V.[8] Cyclic voltammograms of samples were recorded in CH_2Cl_2 (1.0×10^{-3} M) containing N*n*Bu_4PF_6 (0.10 M) using a glassy carbon (GC) working electrode, a Pt wire counter electrode, an Ag/AgCl reference electrode, and a Fc/Fc^+ external standard at room temperature with a scan rate of 0.1 V s^{-1}.

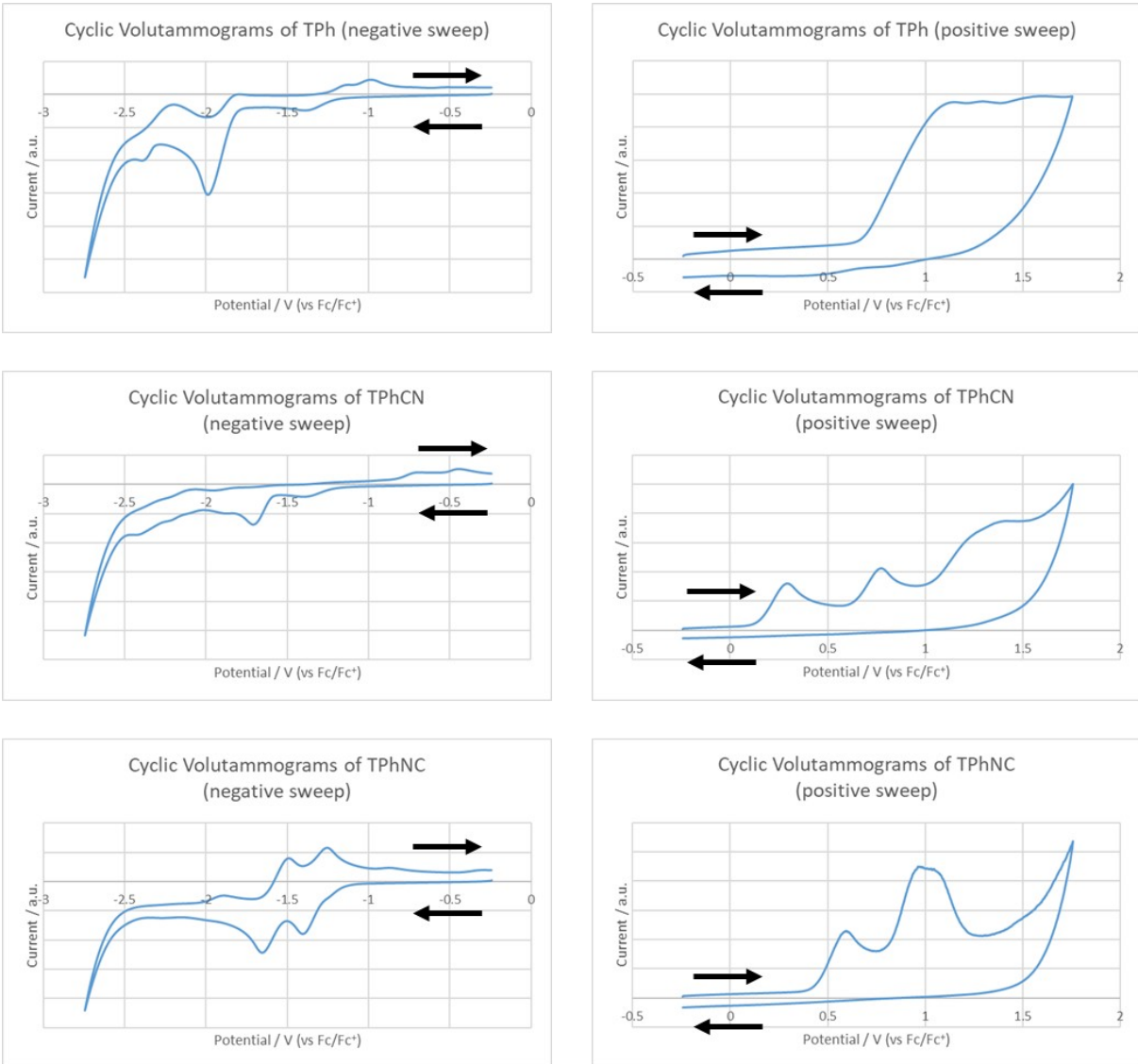

Figure S10. Cyclic voltammograms of **TPh**, **TPhCN**, and **TPhNC** in CH_2Cl_2 (1.0×10^{-3} M). The black arrows denote sweep directions.

Solid state emission

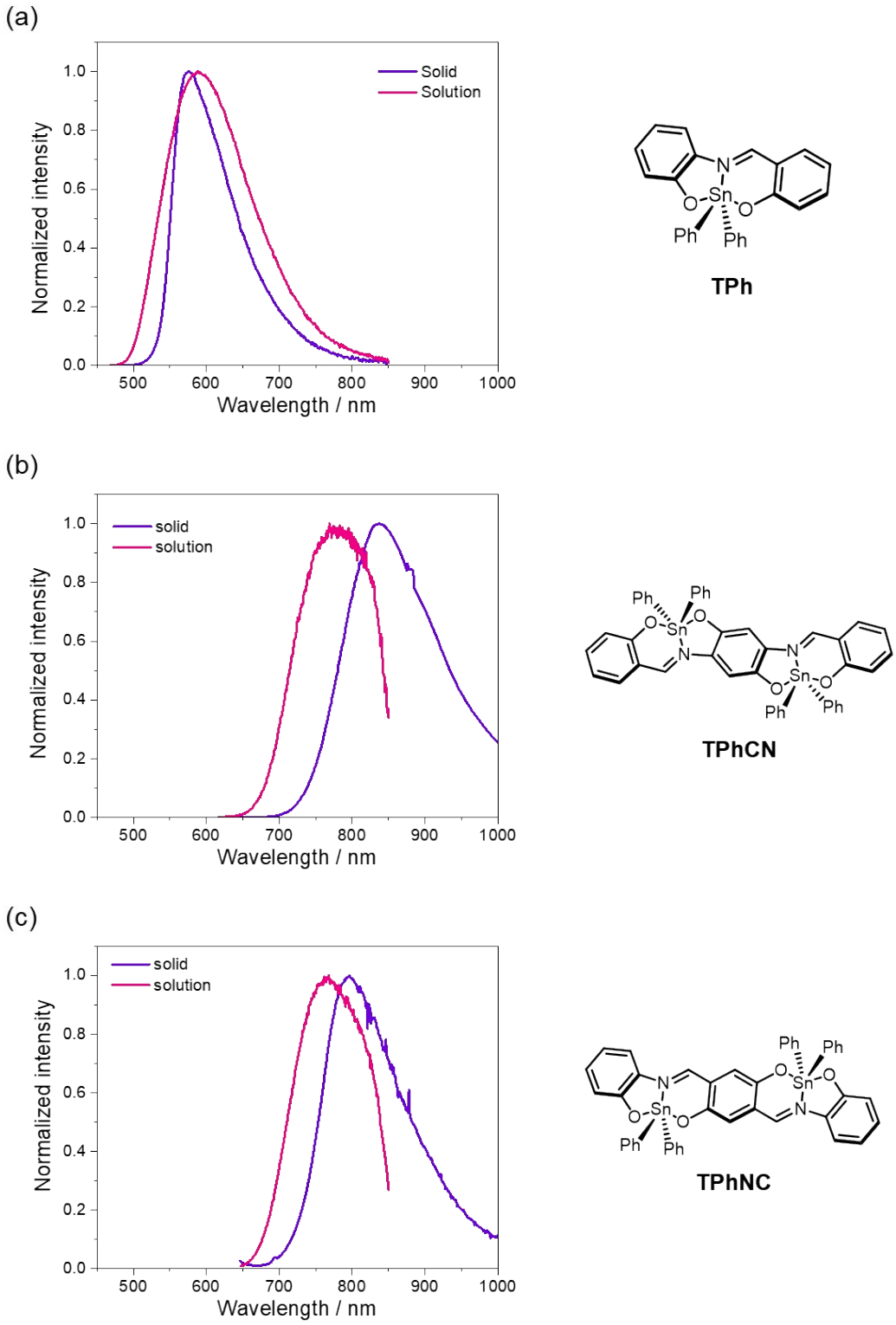

Figure S11. Photoluminescence spectra of (a) **TPh**, (b) **TPhCN**, and (c) **TPhNC** in solution (toluene, 1.0×10^{-5} M) and solid state (with PMT P928 (250~810 nm) and DSS-IGA (810~1550 nm) as detectors only in solid state).

Solvent-dependent optical properties of TPh derivatives

Table S9. Solvent-dependent optical properties of TPh derivatives

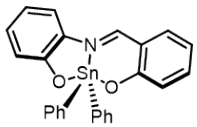

TPh

	λ_{abs} [a] /nm	ε [a] /10^5 cm^{-1} M^{-1}	λ_{PL} [a] /nm	Φ_{FL} [b] /%
c-hex	461	0.127	578	26.5
toluene	454	0.129	584	23.9
$CHCl_3$	454	0.127	587	20.4
CH_2Cl_2	453	0.132	589	16.9

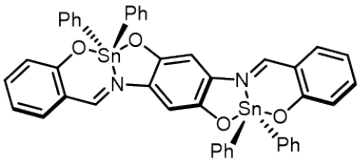

TPhCN

	λ_{abs} [a] /nm	ε [a] /10^5 cm^{-1} M^{-1}	λ_{PL} [a] /nm	Φ_{FL} [b] /%
c-hex	612	0.254	776	0.6
toluene	602	0.268	776	0.6
$CHCl_3$	598	0.275	775	0.8
CH_2Cl_2	595	0.279	777	0.5

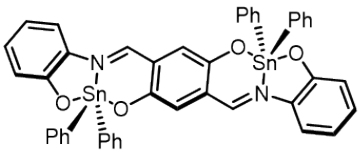

TPhNC

	λ_{abs} [a] /nm	ε [a] /10^5 cm^{-1} M^{-1}	λ_{PL} [a] /nm	Φ_{FL} [b] /%
c-hex	643	0.157	768	3.4
toluene	631	0.166	767	3.3
$CHCl_3$	629	0.159	773	2.2
CH_2Cl_2	624	0.157	772	2.6

[a]In toluene/each solvent = 1/99 v/v (1.0×10^{-5} M per repeating unit). [b]Absolute FL quantum yield, excited at absorption maxima for **TPh** and at 525 nm for **TPhCN** and **TPhNC**.

Computational details for theoretical calculation for solvent effects

The Gaussian 16 program package[10] was used for computation. We optimized the structures of **TPh**, **TPhCN**, and **TPhNC** in the ground S_0 states and calculated their orbitals. The DFT was applied to optimize the structures in the S_0 states at B3LYP/6-31G(d) for C, H, N, O and LanL2DZ for Sn. We calculated the energy of the S_0–S_1 transitions with optimized geometries in the S_0 states by time-dependent (TD)-DFT at B3LYP/6-31G(d) for C, H, N, O and LanL2DZ for Sn. Solvent effects were evaluated by using the default setting (scrf).

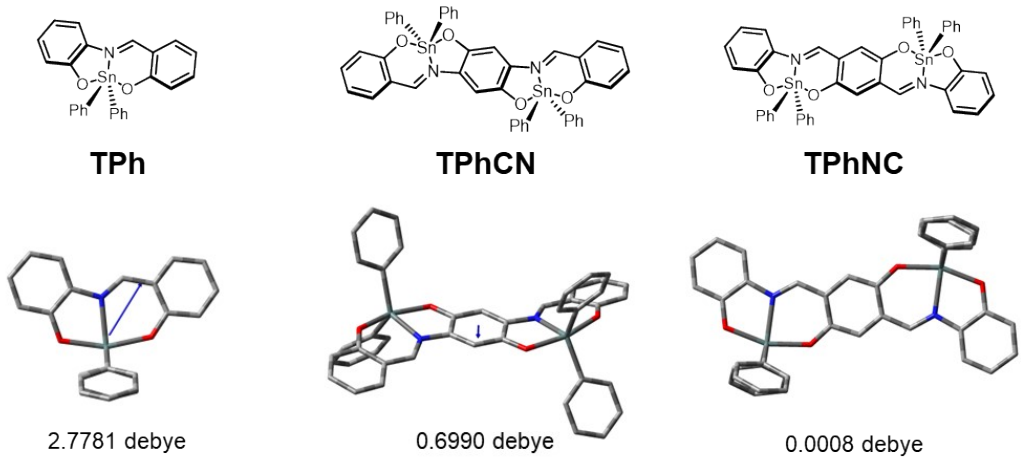

Figure S12. Optimized structures and dipole moments of TPh derivatives.

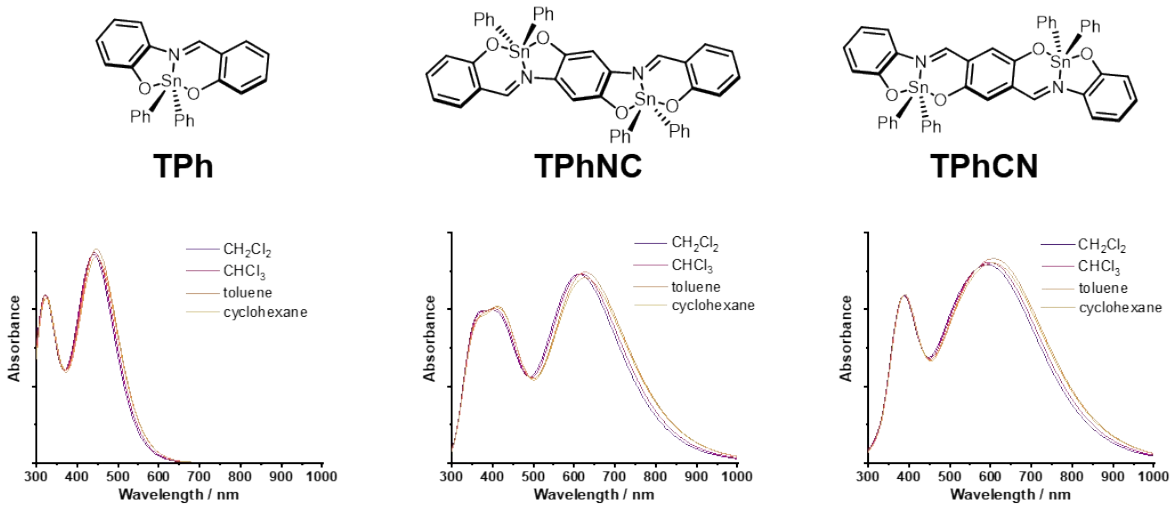

Figure S13. Predicted solvent-dependent absorption spectra of TPh derivatives obtained from DFT calculation.

Solvent-dependent optical properties of polymers

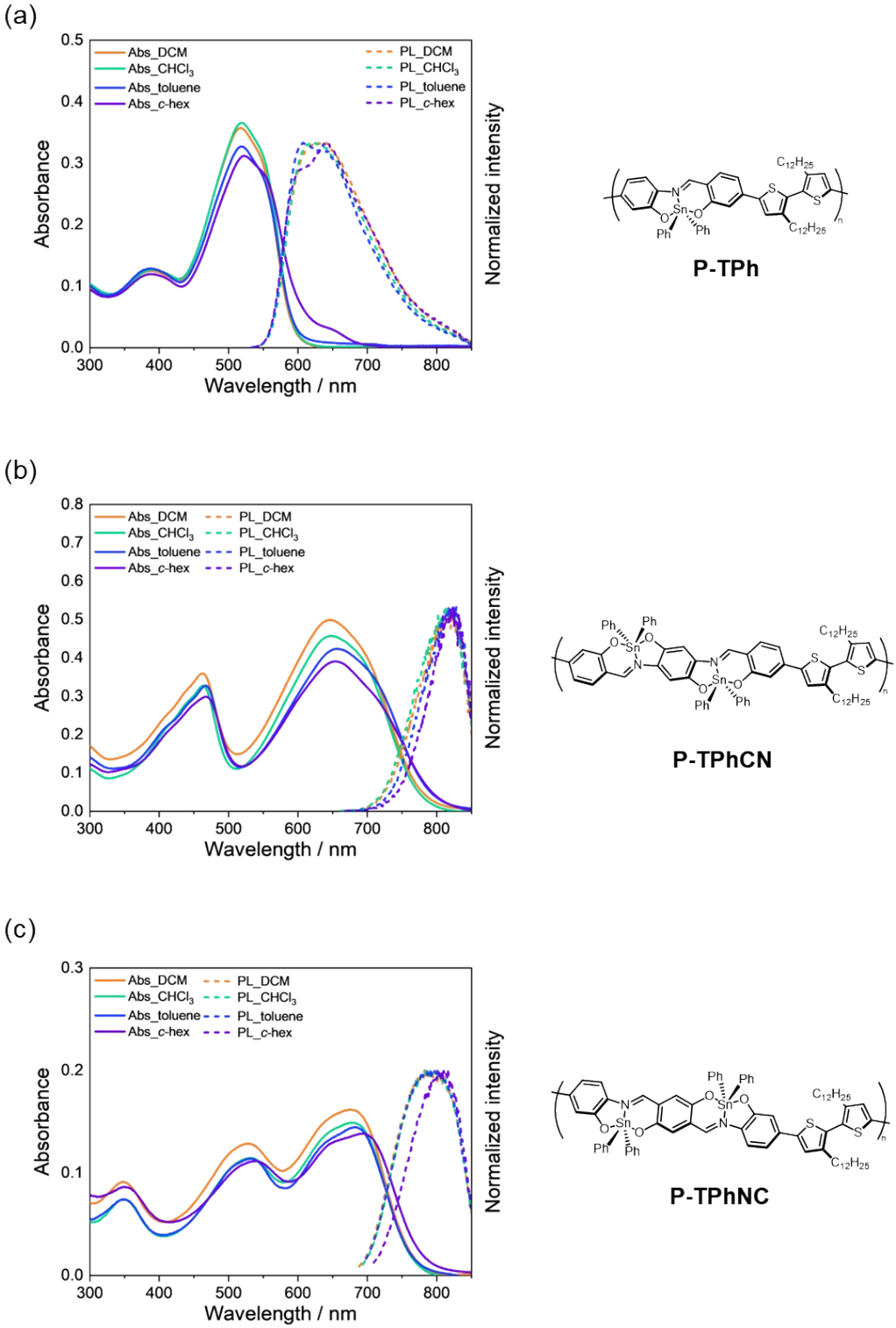

Figure S14. Solvent-dependent UV–vis absorption and fluorescence spectra of (a) **TPh**, (b) **TPhCN**, and (c) **TPhNC** in each solvent (1.0×10^{-5} M per repeating unit, $CHCl_3$/each solvent = 1/99 v/v).

Table S10. Solvent dependent optical properties of conjugated polymers

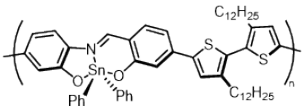

P-TPh

	λ_{abs} [a] /nm	ε [a] /10^5 cm^{-1} M^{-1}	λ_{PL} [a] /nm	Φ_{FL} [b] /%
c-hex	523	0.312	640	23.4
toluene	519	0.327	607	33.8
$CHCl_3$	518	0.366	621	35.8
CH_2Cl_2	518	0.357	637	31.1

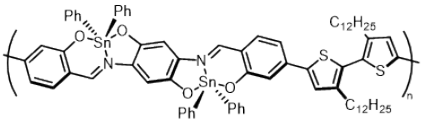

P-TPhCN

	λ_{abs} [a] /nm	ε [a] /10^5 cm^{-1} M^{-1}	λ_{PL} [a] /nm	Φ_{FL} [b] /%
c-hex	653	0.391	824	0.2
toluene	658	0.427	828	0.3
$CHCl_3$	647	0.457	817	0.4
CH_2Cl_2	647	0.499	818	0.3

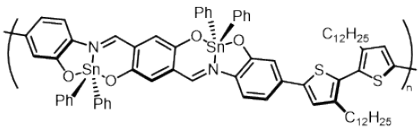

P-TPhNC

	λ_{abs} [a] /nm	ε [a] /10^5 cm^{-1} M^{-1}	λ_{PL} [a] /nm	Φ_{FL} [b] /%
c-hex	694	0.139	808	0.9
toluene	683	0.145	801	1.2
$CHCl_3$	678	0.149	792	1.1
CH_2Cl_2	673	0.162	796	0.8

[a]In $CHCl_3$/each solvent = 1/99 v/v (1.0×10^{-5} M per repeating unit), excited at λ_{abs} for FL. [b]Absolute FL quantum yield, excited at 518 nm for **P-TPh** and 525 nm for **P-TPhCN** and **P-TPhNC**.

Optical properties of polymers in film state

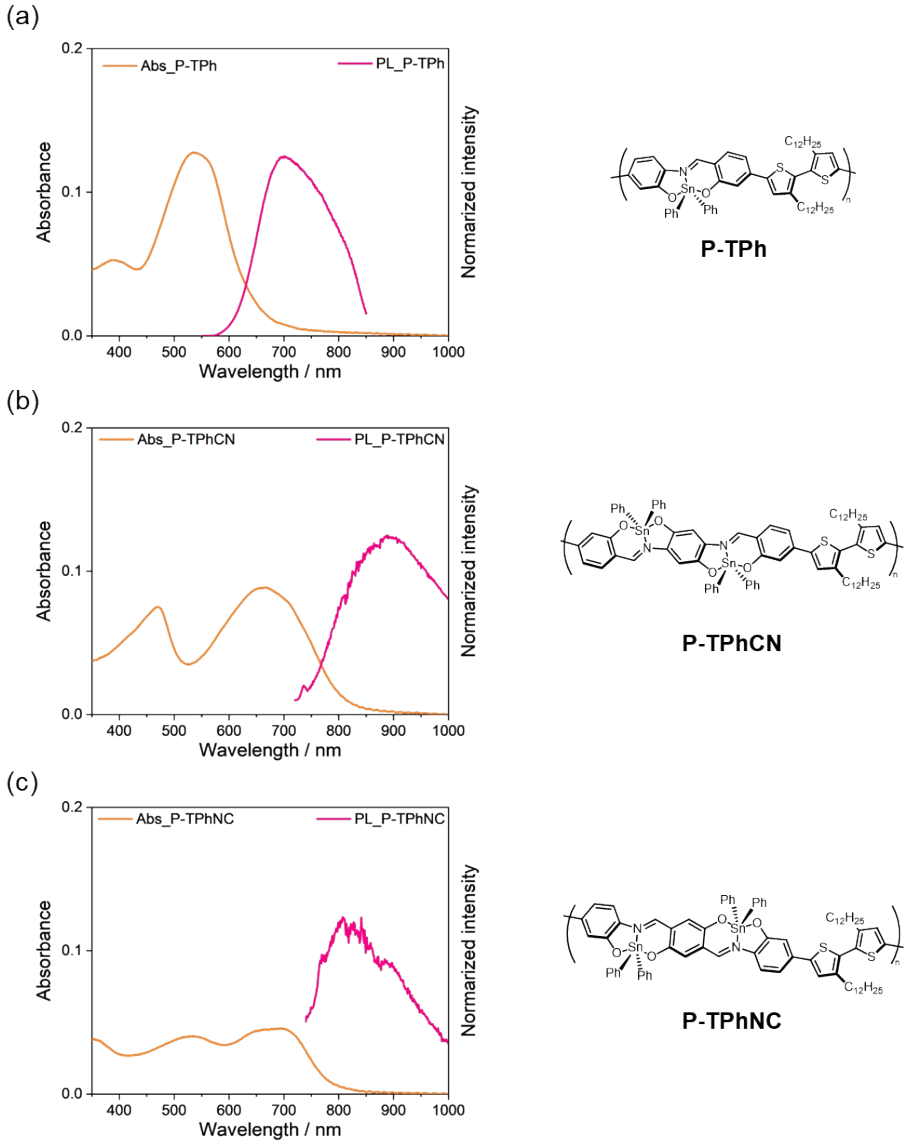

Figure S15. UV–vis absorption and fluorescence spectra of (a) **TPh**, (b) **TPhCN**, and (c) **TPhNC** as a spin-coated film (1 mg / 300 μL for **P-TPh**, saturated solution for **P-TPhCN** and **P-TPhNC** in $CHCl_3$).

Table S11. Solvent-dependent optical properties of conjugated polymers

	λ_{abs} [a] /nm	λ_{PL} [a] /nm	Φ_{FL} [b] /%
P-TPh	536	701	3.5
P-TPhCN	667	889	0.3
P-TPhNC	696	807	0.3

[a]Spin-coated film (1 mg / 300 μL for **P-TPh**, saturated solution for **P-TPhCN** and **P-TPhNC** in $CHCl_3$), excited at λ_{abs} for FL. [b]Absolute FL quantum yield, excited at 536 nm for **P-TPh** and 525 nm for **P-TPhCN** and **P-TPhNC**.

Computational details for theoretical calculation for CPs

The Gaussian 16 program package[10] was used for computation. We optimized the structures of **TPh**, ***di*-TPh**, ***tri*-TPh**, **TPhCN**, ***di*-TPhCN**, ***tri*-TPhCN**, **TPhNC**, ***di*-TPhNC**, and ***tri*-TPhNC** in the ground S_0 states and calculated their orbitals. The DFT was applied to optimize the structures in the S_0 states at B3LYP/6-31G(d) for C, H, N, O and LanL2DZ for Sn. We calculated the energy of the S_0–S_1 transitions with optimized geometries in the S_0 states by time-dependent (TD)-DFT at B3LYP/6-31G(d) for C, H, N, O, S and LanL2DZ for Sn.

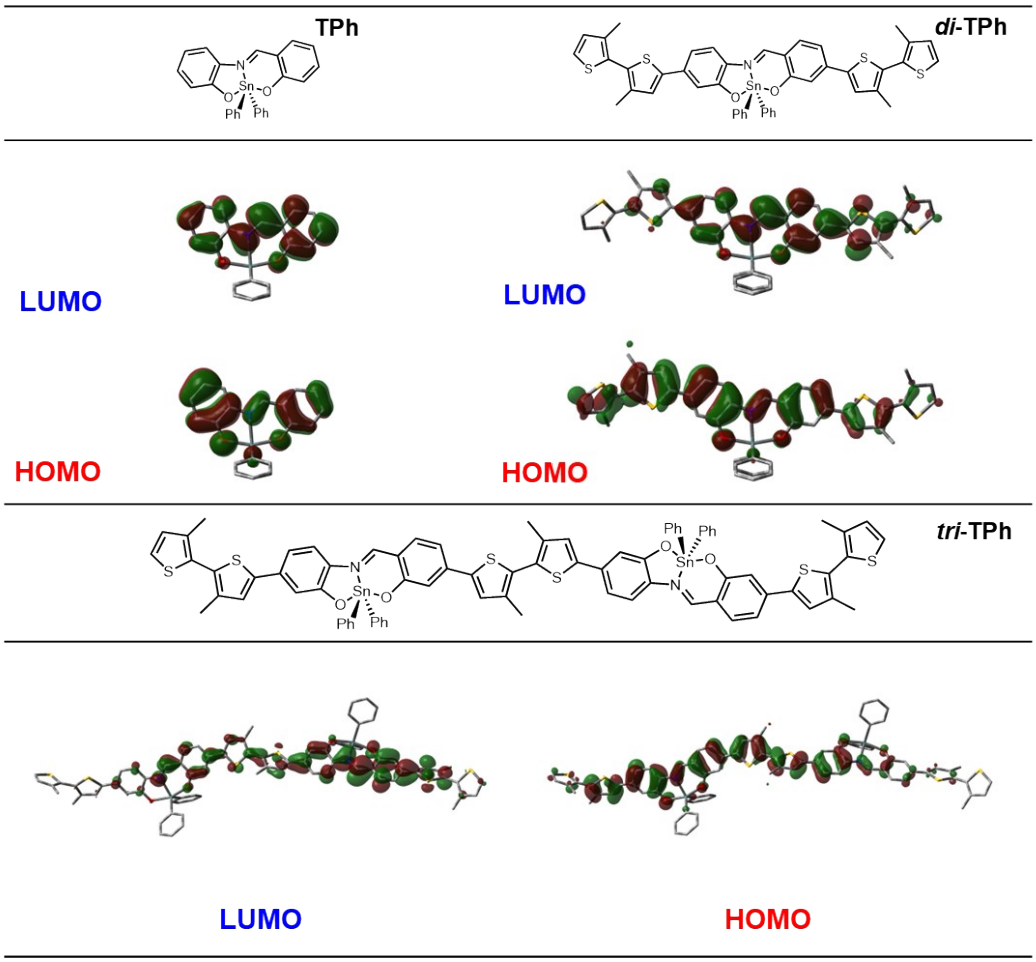

Figure S16. Chemical structures, HOMOs, and LUMOs of **TPh**, ***di*-TPh**, and ***tri*-TPh**.

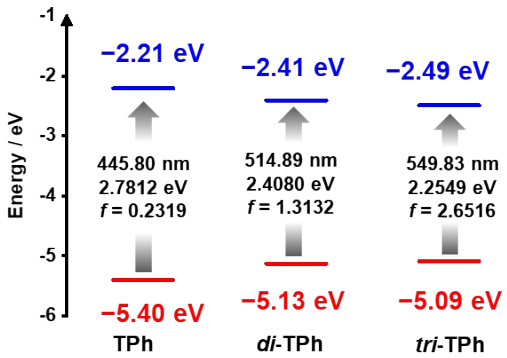

Figure S17. Calculated energy diagrams and S_0–S_1 transition energies of **TPh**, ***di*-TPh**, and ***tri*-TPh**.

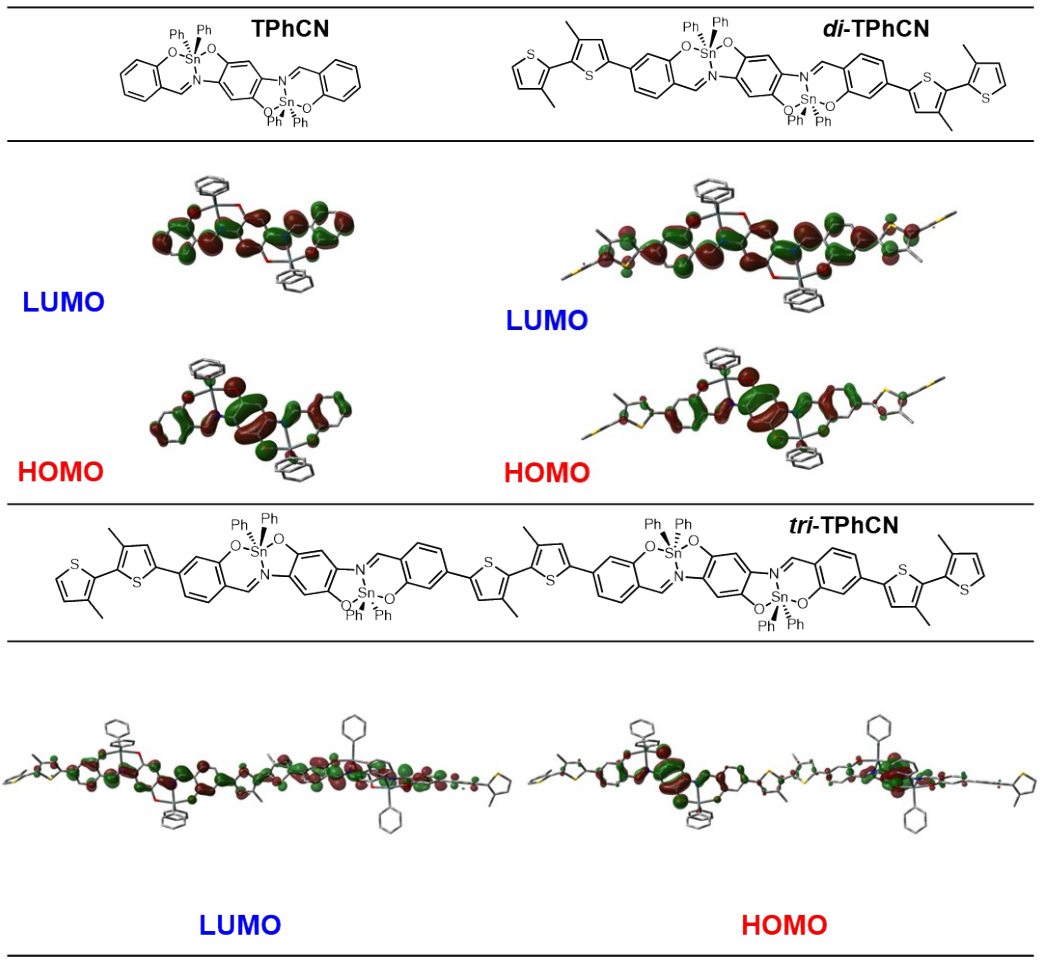

Figure S18. Chemical structures, HOMOs, and LUMOs of **TPhCN**, ***di*-TPhCN**, and ***tri*-TPhCN**.

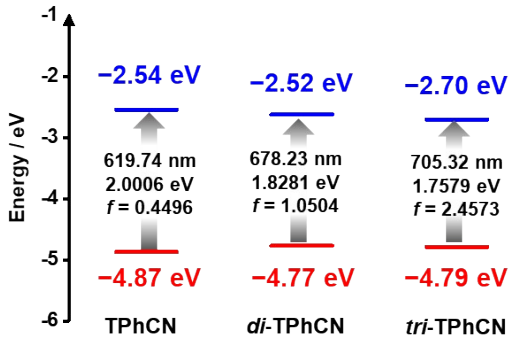

Figure S19. Calculated energy diagrams and S_0–S_1 transition energies of **TPhCN**, ***di*-TPhCN**, and ***tri*-TPhCN**.

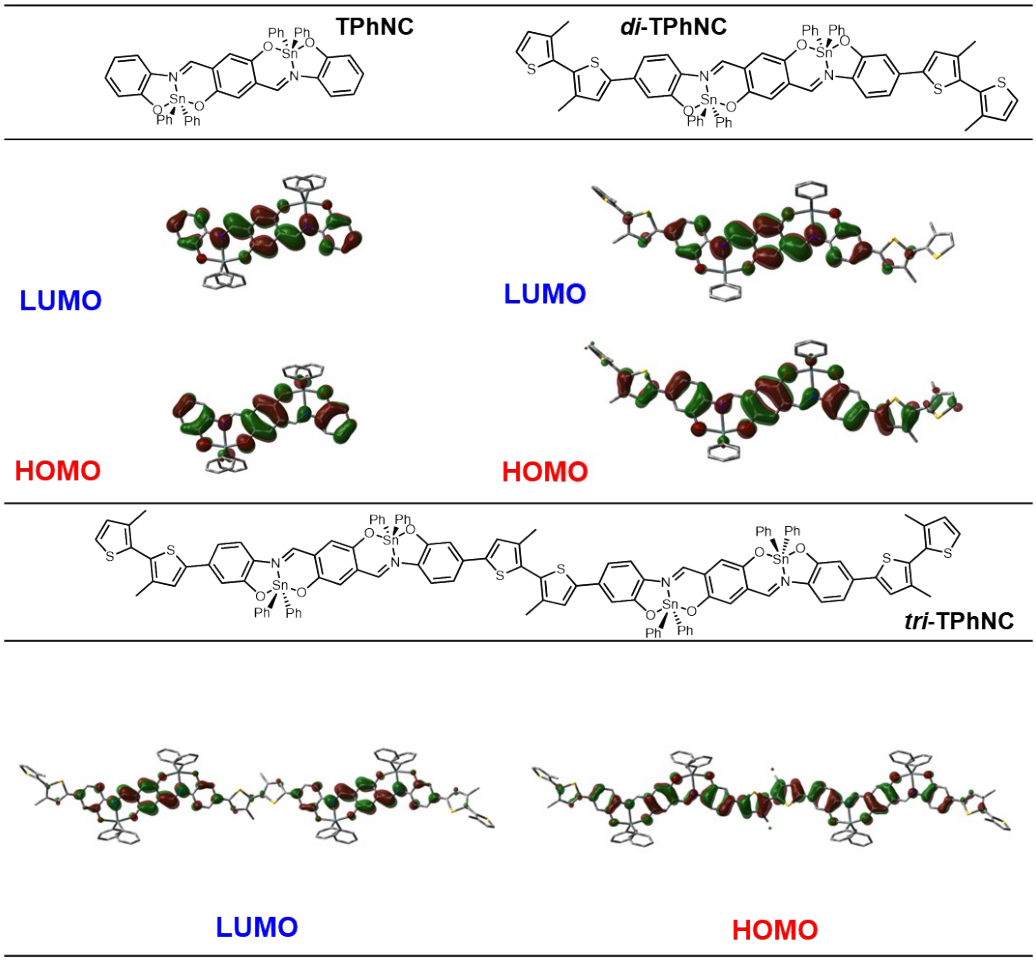

Figure S20. Chemical structures, HOMOs, and LUMOs of **TPhNC**, ***di*-TPhNC**, and ***tri*-TPhNC**.

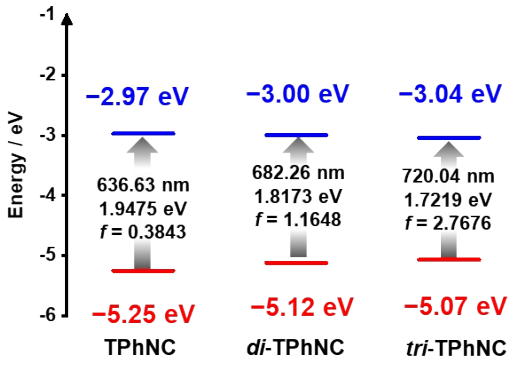

Figure S21. Calculated energy diagrams and S_0–S_1 transition energies of **TPhNC**, ***di*-TPhNC**, and ***tri*-TPhNC**.

References

[1] Rigaku. REQAB. Program for Absorption Correction. Rigaku Corporation, Tokyo, Japan, **1998**.

[2] G. M. Sheldrick, *Acta Crystallogr. Sect. A: Found. Adv.* **2015**, *71*, 3–8.

[3] G. M. Sheldrick, *Acta Crystallogr. Sect. A: Found. Crystallogr.* **2008**, *64*, 112–122.

[4] G. M. Sheldrick, *Acta Crystallogr. Sect. C: Struct. Chem.* **2015**, *71*, 3–8.

[5] G. M. Sheldrick, SHELXL-2018. Programs for Crystal Structure Analysis.; Universität Göttingen, Göttingen, Germany, **2018**.

[6] K. Wakita, Yadokari&XG. Program for Crystal Structure Analysis.; **2000**.

[7] L. J. Farrugia, ORTEP-3 for Windows-a Version of ORTEP-III with a Graphical User Interface (GUI), *J. Appl. Cryst.*, **1997**, *30*, 565.

[8] a) C. M. Cardona, W. Li, A. E. Kaifer, D. Stockdale, G. C. Bazan, *Adv. Mater.* **2011**, *23*, 2367-2371; b) J. Pommerehne, H. Vestweber, W. Guss, R. F. Mahrt, H. Bässler, M. Porsch, J. Daub, *Adv. Mater.* **1995**, *7*, 551-554.

[9] J. S. Zugazagoitia, M. Maya, C. Damián-Zea, P. Navarro, H. I. Beltran and J. Peon, *J. Phys. Chem A*, **2010**, *114*, 704–714.

[10] Gaussian 16, Revision A.03, M. J. Frisch, G. W. Trucks, H. B. Schlegel, G. E. Scuseria, M. A. Robb, J. R. Cheeseman, G. Scalmani, V. Barone, G. A. Petersson, H. Nakatsuji, X. Li, M. Caricato, A. V. Marenich, J. Bloino, B. G. Janesko, R. Gomperts, B. Mennucci, H. P. Hratchian, J. V. Ortiz, A. F. Izmaylov, J. L. Sonnenberg, D. Williams-Young, F. Ding, F. Lipparini, F. Egidi, J. Goings, B. Peng, A. Petrone, T. Henderson, D. Ranasinghe, V. G. Zakrzewski, J. Gao, N. Rega, G. Zheng, W. Liang, M. Hada, M. Ehara, K. Toyota, R. Fukuda, J. Hasegawa, M. Ishida, T. Nakajima, Y. Honda, O. Kitao, H. Nakai, T. Vreven, K. Throssell, J. A. Montgomery, Jr., J. E. Peralta, F. Ogliaro, M. J. Bearpark, J. J. Heyd, E. N. Brothers, K. N. Kudin, V. N. Staroverov, T. A. Keith, R. Kobayashi, J. Normand, K. Raghavachari, A. P. Rendell, J. C. Burant, S. S. Iyengar, J. Tomasi, M. Cossi, J. M. Millam, M. Klene, C. Adamo, R. Cammi, J. W. Ochterski, R. L. Martin, K. Morokuma, O. Farkas, J. B. Foresman, and D. J. Fox, Gaussian, Inc., Wallingford CT, **2016**.